

1 **A Regional multi-Air Pollutant Assimilation System (RAPAS v1.0)**
2 **for emission estimates: Ssystem development and application**

3 Shuzhuang Feng¹, Fei Jiang^{1,2}, Zheng Wu³, Hengmao Wang^{1,2}, Wei He¹, Yang Shen¹,
4 Lingyu Zhang¹, Yanhua Zheng¹, Chenxi Lou¹, Ziqiang Jiang⁴, Weimin Ju^{1,2}

5
6 ¹ *Jiangsu Provincial Key Laboratory of Geographic Information Science and Technology, International*
7 *Institute for Earth System Science, Nanjing University, Nanjing, 210023, China*

8 ² *Jiangsu Center for Collaborative Innovation in Geographical Information Resource Development and*
9 *Application, Nanjing, 210023, China*

10 ³ *Chongqing Institute of Meteorological Sciences, Chongqing, 401147, China*

11 ⁴ *Jiangsu Environmental Monitoring Center, Nanjing, 210019, China*

12
13
14
15
16 *Correspondence to: Fei Jiang (jiangf@nju.edu.cn)*

30 Abstract

31 Top-down atmospheric inversion infers surface-atmosphere fluxes from spatially
32 distributed observations of atmospheric compositions, which is a vital means for
33 quantifying ~~large-scale~~ anthropogenic and natural emissions. In this study, we
34 developed a Regional multi-Air Pollutant Assimilation System (RAPAS v1.0) based on
35 the Weather Research and Forecasting/Community Multiscale Air Quality Modelling
36 System (WRF/CMAQ) model, the three-dimensional variational (3DVAR) algorithm,
37 and the ensemble square root filter (EnSRF) algorithm. ~~It is capable of~~ This system can
38 simultaneously ~~assimilating~~ assimilate ~~spatially distributed~~ hourly ~~in situ~~ in situ
39 ~~measurements of~~ CO, SO₂, NO₂, PM_{2.5} and PM₁₀ ~~concentrations~~ observations to
40 ~~quantitatively optimize~~ infer gridded emissions of CO, SO₂, NO_x, primary PM_{2.5}
41 (PPM_{2.5}), and coarse PM₁₀ (PMC) on a regional scale. In each data assimilation window,
42 ~~we use a~~ RAPAS includes two subsystems, initial field assimilation (IA) subsystem and
43 ~~emission inversion (EI) subsystem, which are used to generate a good chemical initial~~
44 ~~condition (IC), and conduct inversions of anthropogenic emissions, respectively. A~~
45 ~~“two-step” inversion scheme is adopted in the EI subsystem in each data assimilation~~
46 ~~(DA) window,~~ in which the emission is inferred ~~in the first step,~~ and then, ~~it is~~ input
47 into the CMAQ model to simulate ~~the~~ initial condition (initial field IC) of the next
48 window, ~~meanwhile, it is also.~~ The posterior emission is transferred to the next window
49 as the prior emission. ~~The chemical IC is optimized through the IA subsystem,~~ and the
50 original emission inventory is only used in the first ~~DA~~ window. ~~Besides~~ Additionally,
51 a “super-observation” approach is implemented ~~based on optimal estimation theory~~ to
52 decrease the computational costs ~~and,~~ observation error correlations, and ~~reduce the~~
53 influence of representativeness errors.

54 ~~With~~ Using this system, we estimated the emissions of CO, SO₂, NO_x, PPM_{2.5} and
55 PMC in December and July 2016 over China using ~~the corresponding~~ nationwide
56 surface observations. ~~The 2016 Multi-resolution Emission Inventory for China (MEIC~~
57 ~~2016) was used as the prior emission. For December, the system was run from 26~~
58 ~~November to 31 December, in which the IA subsystem was run in the first 5 days, and~~

59 ~~the EI subsystem was run in the following days. In July, the system was run in the same~~
60 ~~way. The evaluation and sensitivity testing of this system mainly focused on December.~~
61 ~~The r~~Results showed that ~~compared to the prior emissions (MEIC 2016), the posterior~~
62 ~~emissions of CO, SO₂, NO_x, PPM_{2.5}, and PMC in December 2016 increased by 129%,~~
63 ~~20%, 5%, 95%, and 1045%, respectively, and the emission uncertainties decreased by~~
64 ~~44%, 45%, 34%, 52%, and 56%, respectively. With the inverted emissions, the~~
65 ~~simulated concentrations of CO, NO₂, SO₂, PM_{2.5} and PM₁₀ with the prior inventory~~
66 ~~have large systematic biases, with relative biases in the range of -48.2-54.2%. In the IA~~
67 ~~subsystem, after 3DVAR, the root mean squared error (RMSE) of the simulated~~
68 ~~concentrations decreased by 50.0-73.2%, and the correlation coefficient (CORR)~~
69 ~~increased to 0.78-0.92 for the five species. In the EI subsystem, after emission~~
70 ~~inversions, the RMSE of the simulated concentrations decreased by 40.1-56.3%, and~~
71 ~~the CORR increased to 0.69-0.87. For the whole mainland China, the uncertainties were~~
72 ~~reduced by 44.4%, 45.0%, 34.3%, 51.8% and 56.1% for CO, SO₂, NO_x, PPM_{2.5} and~~
73 ~~PMC, respectively. Overall, compared to the prior emission (MEIC 2016), the posterior~~
74 ~~emissions increased by 129%, 20%, 5%, and 95% for CO, SO₂, NO_x and PPM_{2.5},~~
75 ~~respectively, indicating that there was significant underestimation in the MEIC~~
76 ~~inventory. The posterior PMC emissions, including anthropogenic and natural dust~~
77 ~~contributions, increased by 1045%. A series of s~~Sensitivity tests were conducted with
78 different inversion processes, prior emissions, prior uncertainties, and observation
79 errors. ~~The r~~Results showed that the “two-step” scheme ~~clearly~~ outperformed the
80 simultaneous assimilation of ICs and emissions (~~“one-step” scheme~~) ~~in emission~~
81 ~~inversion,~~ and the system ~~is rather~~is robust in estimating ~~the~~ emissions using ~~the~~
82 nationwide surface observations over China. ~~Our~~ ~~This~~ study offers a useful tool for
83 accurately quantifying multi-species anthropogenic emissions at large scales and ~~in~~
84 near ~~_~~real time.

88 1. Introduction

89 ~~Due Owing~~ to rapid economic developments and pollution control legislations, there is
90 an increasing demand to provide updated emission estimates ~~has arisen~~, especially in
91 areas where anthropogenic emissions are intensive. Accurately estimating source
92 emission quantities and spatiotemporal changes resulting from various regulations is
93 imperative and valuable for understanding air quality responses and is crucial for
94 providing timely instructions for the design of future emissions regulations. However,
95 most inventories ~~have been were~~ developed based on a bottom-up approach and are
96 usually updated with a delay of a few years ~~a few years delay owing due~~ to the
97 complexity of gathering ~~all~~ statistical information on activity levels and sector-specific
98 emission factors (Ding et al., 2015). The large uncertainty associated with the low
99 temporal and spatial resolutions of these datasets also greatly limits the assessment of
100 emission changes. Some studies (Bauwens et al., 2020; Shi and Brasseur, 2020) have
101 evaluated emission changes indirectly through concentration measurements, ~~but;~~
102 however, air pollution changes are not only dominated by emission changes, but also
103 highly affected by meteorological conditions (Shen et al., 2021).

104 Top-down atmospheric inversion infers surface-atmosphere fluxes from spatially
105 distributed observations of atmospheric compositions. Recent efforts have focused on
106 developing air pollution data assimilation (DA) systems to conduct ~~the~~ top-down
107 inversions, which is able to can integrate model and multi-source ~~and large amounts of~~
108 observational information to constrain emission sources. Two major methods, ~~namely,~~
109 ~~4D-variational data assimilation (4DVAR) and ensemble Kalman filter (EnKF),~~ are
110 widely used in those DA systems: 4D-variational data assimilation (4DVAR) and
111 ensemble Kalman filter (EnKF). 4DVAR provides a global optimal analysis ~~through by~~
112 minimizing a cost function. It shows an implicit flow-dependent background error
113 covariance and can reflect complex nonlinear constraint relationships (Lorenc, 2003).
114 Additionally, a weak constraint 4DVAR method ~~the model error~~ can ~~be~~ partly accounted
115 for the model error with a weak constraint 4DVAR method through the by defining
116 ~~definition of~~ a systematic error term in a cost function (Derber, 1989). For example, the

117 GEOS-Chem and TM5 4DVAR frameworks have been used to estimate CH₄ (Alexe et
118 al., 2015; [Monteil et al., 2013](#); Schneising et al., 2009; Stanevich et al., 2021; Wecht et
119 al., 2014) and CO₂ fluxes (Basu et al., 2013; Nassar et al., 2011; Wang et al., 2019a)
120 from different satellite retrieval products. ~~Monteil et al. (2013) showed that the global
121 patterns of CH₄ emissions derived from SCIAMACHY (with bias correction) and
122 GOSAT retrievals are in remarkable agreement based on 15 months observations.~~
123 Additionally, Jiang et al. (2017) ~~and Stavrakou et al. (2008)~~ [Kurokawa et al. \(2009\)](#) also
124 used the 4DVAR algorithm to ~~_~~estimate global CO ~~and NO_x~~ emission trends ~~from~~
125 ~~2000–2015~~ using MOPITT ~~and GOME/SCIAMACHY~~ retrievals, ~~respectively.~~
126 ~~Kurokawa et al. (2009) and Stavrakou et al. (2008) also used the 4DVAR technique to~~
127 ~~estimate NO_x emission. Using NIES LiDAR observations, Yumimoto et al. (2008)~~
128 ~~applied the 4DVAR DA to infer dust emissions over eastern Asia and the results agreed~~
129 ~~well with various satellite data and surface observations. Based on surface observations,~~
130 ~~Meirink et al. (2008) developed a 4DVAR system to optimize monthly methane~~
131 ~~emissions, which showed a high degree of consistency in posterior emissions and~~
132 ~~uncertainties when compared with an analogous inversion based on the traditional~~
133 ~~synthesis approach. Changes.~~
134 Although considerable progress has been made to reduce large uncertainties in emission
135 inventories, tThe drawback of the 4DVAR method is the additional development of
136 adjoint models, which ~~that~~ are technically difficult and cumbersome for complex
137 chemical transport models ([Bocquet and Sakov, 2013](#)). Instead, EnKF uses ~~the~~ flow-
138 dependent background error covariance generated by ensemble simulations to map ~~the~~
139 deviations in concentrations to increments of emissions, which is more flexible and
140 easier to implement. Many previous studies ~~have~~ used EnKF techniques to assimilate
141 ~~the~~ single- or dual- species observations to optimize the corresponding emission species
142 (Chen et al., 2019; Peng et al., 2017; Schwartz et al., 2014; Sekiyama et al., 2010).
143 Miyazaki et al. (2017) improved NO_x emission estimates using multi-constituent
144 satellite observations, and further estimated global surface NO_x emissions from 2005 to
145 2014. Feng et al., (2020b) used surface observations of NO₂ to infer the NO_x emission

146 changes in China during the COVID-19, and quantitatively evaluate the impact of the
147 epidemic on economic activities from the perspective of emission change. Tang et al.
148 (2011) reported that the simultaneous optimizations of the ICs of O₃, NO_x and volatile
149 organic compounds (VOCs) and adjusted the emissions of NO_x and VOCs through
150 assimilating surface O₃ observations and achieved produced an overall better
151 performance in ozone O₃ forecasts than the adjustment in emissions only. However,
152 such a revision may encounter the problem of model error compensation rather than a
153 retrieval of physically meaningful quantities, which should be avoided from overfitting
154 for emission inversion purposes (Bocquet, 2012; Navon, 1998; Tang et al., 2011). The
155 EnKF has also been widely applied to optimize emissions of carbon dioxide (Jiang et
156 al., 2021; Liu et al., 2019), carbon monoxide (Feng et al., 2020a; Mizzi et al., 2018),
157 sulfur dioxide (Chen et al., 2019), ammonia (Kong et al., 2019), etc.

158 Multi-species data assimilation ~~has shown the advantage of~~ can efficiently ~~reducing~~
159 ~~reduce~~ the uncertainty in emission inventories and has led to improvements in air
160 quality forecasting (Ma et al., 2019; Miyazaki et al., 2012b), ~~since as it would offers~~
161 additional constraints on emission estimates through ~~the~~ improvements in related
162 atmospheric fields, chemical reactions, and gas-particle transformations (Miyazaki and
163 Eskes, 2013). Barbu et al. (2009) updated sulfur oxide (SO_x) emissions with SO₂ and
164 sulfate aerosol observations and found that the simultaneous assimilation of both
165 species ~~had performed~~ better ~~performance~~ than assimilating ~~one of~~ them
166 ~~alone~~ separately. Muller and Stavrakou (2005) also found that the simultaneous
167 optimization of the sources of CO and NO_x led to better agreement between simulations
168 and observations compared to the case where only CO observations are used.

169 The deviation in the chemical initial condition (IC) is ~~one of the~~ important sources
170 of error that affects the accuracy of emission inversion, because atmospheric inversion
171 fully attributes the biases in simulated and observed concentrations to ~~the~~ deviations in
172 emissions (Meirink et al., 2006; Peylin et al., 2005). The biases of concentrations would
173 be compensated ~~through by the~~ unreasonable adjustment of pollution emissions without
174 the optimization of ICs (Tang et al., 2013). ~~Tang et al. (2011) reported that the~~

175 ~~simultaneous optimizations of the ICs of O₃, NO_x and volatile organic compounds~~
176 ~~(VOCs) and the emissions of NO_x and VOCs produced an overall better performance~~
177 ~~in ozone forecasts than the adjustment in emissions only.~~ Similar method of
178 simultaneously optimizing chemical ICs and emissions ~~were also~~ has been applied to
179 constraining emissions in many previous studies (Ma et al., 2019; Miyazaki et al., 2012a;
180 Peng et al., 2018). For example, Elbern et al. (2007) adjusted O₃ ICs, NO_x ICs and
181 emissions, VOCs ICs and emissions jointly through assimilating surface O₃ and NO_x
182 observations. Although the forecast skills of O₃ were improved, due to the coarse model
183 resolution and the strong nonlinear relationship between O₃ and NO_x, the assimilation
184 of O₃ observation worsened emission inversion and forecast of NO_x. Peng et al. (2018)
185 assimilated near-surface observations to simultaneously optimize the ICs and emissions.
186 In the 72-hr forecast evaluation, their resultant emission succeeded in improving SO₂
187 forecast while having little influence on CO and aerosol forecast and even degrading
188 the forecast of NO₂. Ma et al. (2019) also found that the DA benefits for forecast almost
189 disappeared after 72 hr using optimized ICs and emissions. Although a large
190 improvement has been achieved, this method ~~still~~ has great-significant limitations in
191 emission inversion ~~because as~~ the contributions from the emissions and ~~the~~ chemical
192 ICs to the model's biases es are difficult to distinguish (Jiang et al., 2017). In addition, ~~in~~
193 ~~this method,~~ the constraints of the chemical ICs with observations in each assimilation
194 window make the emission inversions ~~are independent~~ between the assimilation
195 windows independent. This, means that if the emission in one window is overestimated
196 or underestimated, it cannot be transferred to the next window for further ~~correcting~~
197 correction and ~~be compensated in the following windows.~~ Considering the
198 importance of emissions in chemical field prediction (Bocquet et al., 2015), the rapid
199 disappearance of the DA benefits seems unrealistic, indicating that simultaneously
200 optimizing chemical ICs and emissions ~~This~~ may result in a systematic bias in the
201 inverted emissions (Jiang et al., 2021).

202 Since 2013, China has deployed an air pollution monitoring network that publishes
203 nationwide and real-time hourly surface ~~atmospheric~~ observations. This dataset

204 provides an opportunity to improve emission estimates using the DA. In this study, a
205 regional multi- air pollutant assimilation system ~~introducing-using~~ 3DVAR and EnKF
206 DA techniques ~~is-was~~ constructed to simultaneously assimilate various surface
207 observations (e.g., CO, SO₂, NO₂, O₃, PM_{2.5} and PM₁₀). Considering the possible
208 shortcomings of the simultaneous optimization method (named ~~as~~ “one-step” method
209 in this study), ~~as~~ mentioned by Jiang et al. (2021), we adopted a “two-step” method (~~Seet.~~
210 ~~3~~) in this system. Unlike the “one-step” method, the ICs of each DA window in the
211 “two-step” method ~~is-were~~ simulated using the posterior emissions of the ~~pervious~~
212 ~~previous~~ DA window. The capabilities of RAPAS ~~in-for~~ reanalysis field generation
213 and emission inversion estimation ~~was-were also~~ evaluated. The robustness of the
214 system was ~~also~~ investigated with different prior inventories, uncertainty settings of ~~the~~
215 prior emissions, and observation errors. The remainder of this paper is organized as
216 follows: ~~in Sect. 2, we~~ Section 2 introduces the DA system and ~~the~~ observation data, ~~and~~
217 ~~in Sect. 3, we~~ Section 3 describes the experimental design, Section 4 presents and
218 discusses ~~t~~ The results of the system performance and sensitivity tests ~~are presented and~~
219 ~~discussed in Sect. 4, and followed by the conclusions in Sect. 5.~~ Section 5 concludes the
220 paper.

221

222 **2. Method and data**

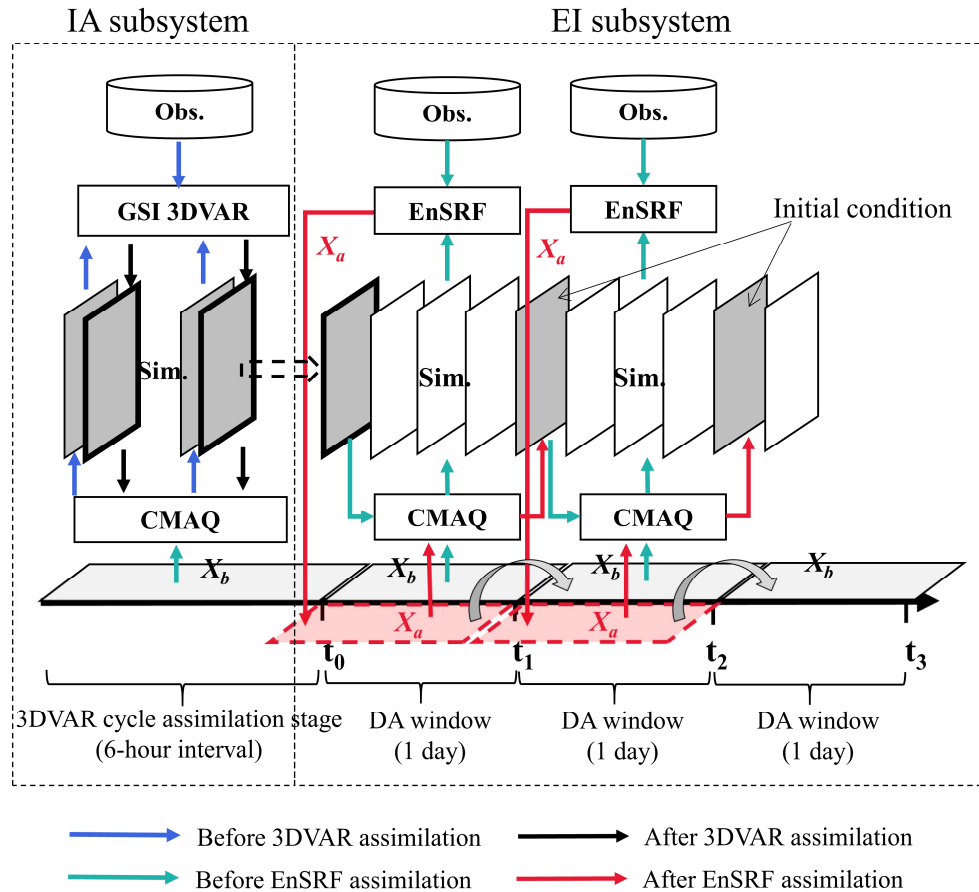
223 **2.1 System description**

224 **2.1.1 Procedure of the assimilation system**

225 A regional air pollutant assimilation system has been preliminarily constructed and
226 successfully applied in our previous studies to optimize the gridded CO and NO_x
227 emissions (Feng et al., 2020a; Feng et al., 2020b). Herein, the system was further
228 extended to simultaneously assimilate multiple species (e.g., CO, SO₂, NO₂, O₃, PM_{2.5},
229 and PM₁₀) and officially named ~~as~~ the Regional multi- Air Pollutant Assimilation
230 System (RAPASv1.0). The RAPAS ~~mainly includes~~ has three components: a regional
231 chemical transport model (CTM), which is coupled offline and used to simulate the

232 meteorological fields and atmospheric compositions, and the 3DVAR and ensemble
233 square root filter (EnSRF) modules, which are used to optimize chemical ICs (Feng et
234 al., 2018; Jiang et al., 2013b) and anthropogenic emissions (Feng et al., 2020a; Feng et
235 al., 2020b), respectively. ~~The introduction of 3DVAR~~ was introduced mainly
236 ~~considering~~ its ~~excellent~~great performance ~~in~~based on our previous study and the
237 lower computational cost during the spin-up period in optimizing ICs. Additionally, ~~it~~
238 ~~has been found that~~ the 3DVAR method can obtain a better IC than the EnKF method
239 (Schwartz et al., 2014).

240 Based on the above three components, the RAPAS ~~is~~was divided into two subsystems;
241 ~~namely~~ the IC assimilation (IA) subsystem (CTM plus 3DVAR) and the emission
242 inversion (EI) subsystem (CTM plus EnSRF). As shown in Figure 1, the IA subsystem
243 ~~is~~was first run to optimize the chemical ICs (Kleist et al., 2009; Wu et al., 2002) for
244 the subsequent EI subsystem. ~~In the IA subsystem, we do not need to d~~Distinguish the
245 ~~type of source~~ types of ~~the~~ model-observation mismatch error was not required for the
246 IA subsystem. The EI subsystem runs cyclically with a “two-step” scheme. In the first
247 step, the prior emissions (X^b) are perturbed and input into the CTM model to simulate
248 chemical concentration ensembles. The simulated concentrations of the lowest model
249 level ~~are~~were then interpolated to the observation space according to the locations and
250 times of the observations using the nearest-~~neighbor~~ interpolation method. ~~The p~~Prior
251 emissions (X^b), simulated observations and real observations ~~are~~were entered into the
252 EnSRF module to generate ~~the~~ optimized emissions (X^a). In the second step, the
253 optimized emissions ~~are~~were re-entered into the CTM model ~~again~~ to generate the ICs
254 of the next DA window. Meanwhile, the optimized emissions ~~are~~were transferred to
255 the next window as ~~the~~ prior emissions. ~~Different from~~Unlike the “one-step” scheme,
256 ~~this~~the “two-step” scheme needs to run the CTM model twice, which is time consuming,
257 but ~~can~~it could transfer the potential errors of the inverted emissions in one DA window
258 to the next for further correction. The benefits of this scheme ~~will~~bear further
259 ~~presented~~discussed in Section- 4.3.



260

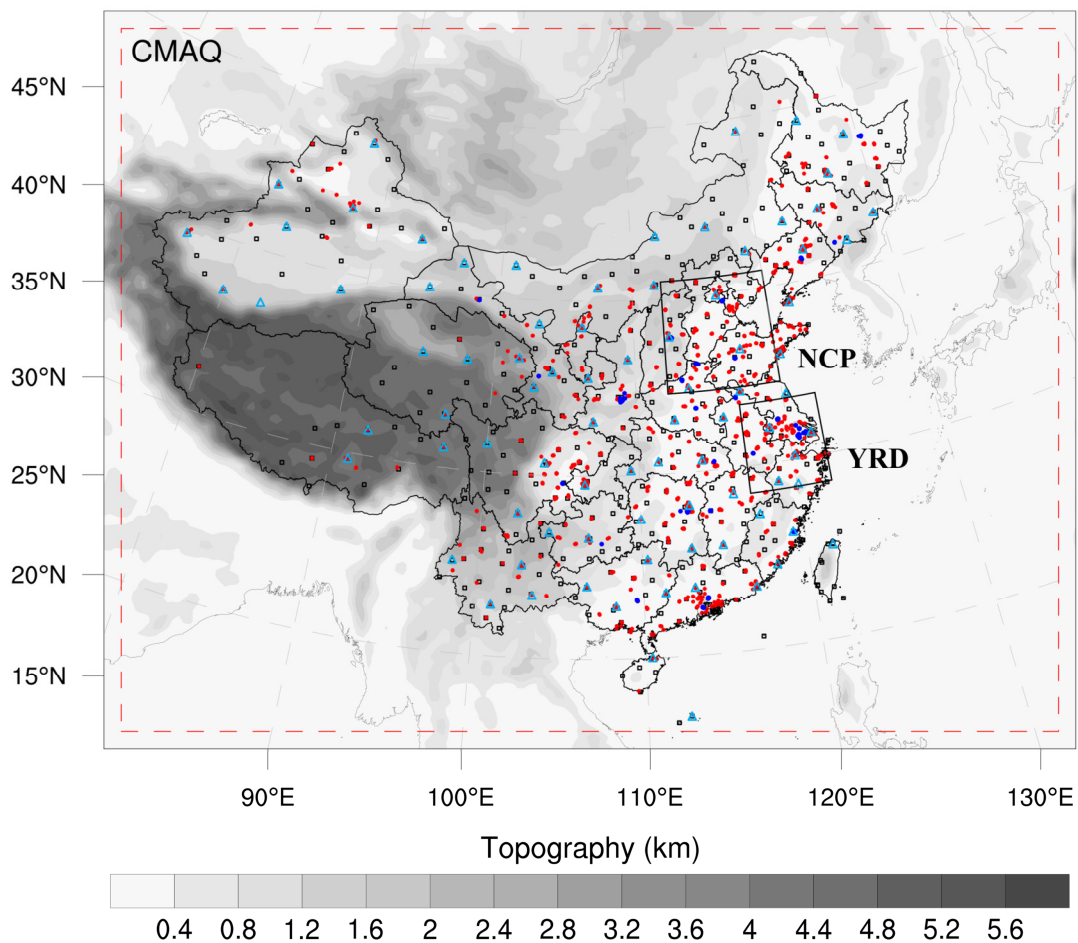
261 **Figure 1.** The composition and flow chart of RAPAS. The x_a and x_b represent the
 262 prior and posterior emissions. The 3DVAR assimilation stage lasts 5 five days with data
 263 input frequency of 6 six hours, and the DA window in the EI subsystem is set to 1 one
 264 day.

265 2.1.2 Atmospheric transport model

266 The regional chemical transport model of Weather Research and
 267 Forecasting/Community Multiscale Air Quality Modelling System (WRF/CMAQ) was
 268 adopted in this study. CMAQ is a regional 3-D Eulerian atmospheric chemistry and
 269 transport model with a “one-atmosphere” design developed in by the US Environmental
 270 Protection Agency (EPA). It can simultaneously address the complex interactions
 271 among multiple pollutants/air quality issues simultaneously. The CMAQ was driven by
 272 the WRF model, which is a state-of-the-art mesoscale numerical weather prediction
 273 system designed for both atmospheric research and meteorological field forecasting. In
 274 this study, WRF version 4.0 and CMAQ version 5.0.2 were adopted used. The WRF

275 simulations were performed with a 36-km horizontal resolution on 169×129 grids, ~~and~~
276 ~~it covering alls the whole~~ of mainland-of China (Figure 2). This spatial resolution has
277 been widely adopted in regional simulations ~~and-as it~~ can provide good simulations of
278 ~~the~~ spatiotemporal variations ~~of-in~~ air pollutants (Mueller and Mallard, 2011; Sharma
279 et al. 2016). In the vertical direction, there ~~are-were~~ 51 sigma levels on ~~the~~ sigma-
280 pressure coordinates extending from the surface to 100 hPa. The underlying surface of
281 ~~the~~ urban and built-up land was replaced by the MODIS land cover retrieval of 2016 to
282 adapt to the rapid expansion of urbanization. The CMAQ model ~~is-was~~ run with the
283 same domain but with three grid cells removed from each side of the WRF domain.
284 There ~~are-were~~ 15 layers in the CMAQ vertical coordinates, which were interpolated
285 from ~~the~~ 51 WRF layers.

286 The meteorological initial and lateral boundary conditions ~~are-were~~ both provided by
287 the Final-(FNL) Operational Global Analysis data of the National Center for
288 Environmental Prediction (NCEP) with a $1^\circ \times 1^\circ$ resolution at 6-h intervals. The
289 chemical lateral boundary conditions and chemical ICs in the IA subsystem ~~come~~
290 ~~originate~~ from ~~the~~ background profiles. As mentioned above, in the EI subsystem, the
291 chemical IC in the first window is provided by the IA subsystem, and in the following
292 windows, it is forward simulated using optimized emissions from the previous window.
293 ~~The~~ Carbon Bond 05 with updated toluene chemistry (CB05tucl) and the 6th generation
294 aerosol module (AERO6) ~~are-were~~ chosen as the gas-phase and aerosol chemical
295 mechanisms, respectively (Appel et al., 2013; Sarwar et al., 2012). ~~The d~~ Detailed
296 physical and chemical configurations are listed in Table 1.



297

298 **Figure 2.** Model domain and observation network. The red dashed frame depicts the
 299 CMAQ computational domain; the black squares represent the surface meteorological
 300 measurement sites; the turquoise triangles represent the sounding sites; and the red and
 301 blue dots represent the air pollution measurement sites. Observations ~~of~~ from all sites
 302 ~~are~~ were assimilated in the 3DVAR subsystem, while observations of city sites where
 303 red dots ~~are~~ were averaged are used for assimilation and where ~~green-blue~~ dots ~~are~~ were
 304 averaged are used for independent evaluation in the EI subsystem; the boxed subregions
 305 are the North China Plain (NCP) and Yangtze River Delta (YRD); and the shaded area
 306 depicts the topography.

307

308

309

310 **Table 1.** Configuration options of WRF/CMAQ

WRF		CMAQ	
Parameter	Scheme	Parameter	Scheme
Microphysics	WSM6	Horizontal/Vertical advection	yamo/wrf
Longwave	RRTM	Horizontal/Vertical diffusion	multiscale/acm2
Shortwave	Goddard	Deposition	m3dry
Boundary layer	ACM	Chemistry solver	EBI
Cumulus	Kain-Fritsch	Photolysis	phot_inline
Land-surface	Noah	Aerosol module	AERO6
Surface layer	Revised	Cloud module	cloud_acm_ae6
Urban canopy	No	Gas-phase chemistry	CB05tucl

311 **2.1.3 3DVAR assimilation algorithm**

312 ~~The~~ Grid-point Statistical Interpolation (GSI) developed ~~in by~~ the US ~~National Centers~~
313 ~~for Environmental Prediction~~ (NCEP) was ~~employed~~ utilized in this study. Building
314 ~~upon~~ the work of Liu et al. (2011), Jiang et al. (2013b) and Feng et al. (2018), we
315 extended ~~it~~ GSI to simultaneously assimilate multiple species (including CO, SO₂, NO₂,
316 O₃, PM_{2.5}, and PM₁₀) and first used individual aerosol species of PM_{2.5} as analysis
317 variables within the GSI/WRF/CMAQ framework. Additional work includes the
318 construction of surface air pollutant observation operators, the updating of observation
319 errors, and the statistics of background error covariance for the analysis variables.
320 Moreover, the data interface was ~~also~~ modified to read/write the CMAQ output/input
321 file directly, which ~~is~~ was easy to implement.

322 In the sense of ~~a~~ minimum analysis error variance, the 3DVAR algorithm optimizes the
323 analysis fields with observations by iterative processes to minimize the cost function
324 (J(x)) defined below:

325
$$J(\mathbf{x}) = \frac{1}{2}(\mathbf{x}_a - \mathbf{x}_b)^T \mathbf{B}^{-1}(\mathbf{x}_a - \mathbf{x}_b) + \frac{1}{2}[H(\mathbf{x}_a) - \mathbf{y}]^T \mathbf{R}^{-1}[H(\mathbf{x}_a) - \mathbf{y}], \quad (1)$$

326 where \mathbf{x}_a is a vector of the analysis field, \mathbf{x}_b ~~denotes is~~ the background field, \mathbf{y} is
327 the vector of observations, \mathbf{B} and \mathbf{R} are the background and observation error
328 covariance matrices, respectively, representing the relative contributions to the
329 analysis, and H is the observation operator that maps the model variables to the
330 observation space.

331 The analysis variables ~~are were~~ the 3D mass concentrations of the pollution
332 ~~compositions components~~ (e.g., CO and sulfate) at each grid point. Hourly mean
333 surface pollution observations within a one+ hour window of the analysis ~~are were~~
334 assimilated. To assimilate the surface pollution observations, model-simulated
335 compositions ~~are were~~ first diagnosed at ~~the~~ observation locations. For gas
336 concentrations ~~that are to be~~ directly used as analysis variables, ~~data the~~ units need to be
337 converted from ppm ~~or and~~ ppb to mg m^{-3} ~~and~~ $\mu\text{g m}^{-3}$, respectively, to match ~~with~~
338 the observations. The model-simulated $\text{PM}_{2.5}$ and PM_{10} concentrations at the ground
339 level ~~are were~~ diagnosed as follows:

$$340 \quad PM_{2.5} = f_i \times PM_i + f_j \times PM_j + f_k \times PM_k = \text{OC} + \text{EC} + \text{SO}_4^{2-} + \text{NO}_3^- + \text{NH}_4^+ + \\ 341 \quad \text{SEAS} + \text{AP}_{2.5} \quad (2)$$

$$342 \quad PM_{10} = PM_i + PM_j + PM_k = PM_{2.5} + \text{PMC} \quad (3)$$

343 where f_i , f_j , and f_k are the $\text{PM}_{2.5}$ fractions of the Aitken, accumulation, and coarse
344 modes, respectively. These ratios are recommended as the concentrations of $\text{PM}_{2.5}$ and
345 fine mode aerosols (i.e., Aitken plus accumulation) ~~could can~~ differ because ~~the~~ $\text{PM}_{2.5}$
346 particles include small tails from the coarse mode in the CMAQ model (Binkowski and
347 Roselle, 2003; Jiang et al., 2006). PM_i , PM_j , and PM_k ~~represent are~~ the mass
348 concentrations of the 3-three modes in the CMAQ model, respectively. Seven aerosol
349 species of $\text{PM}_{2.5}$, ~~including~~ (organic carbon (OC), elemental carbon (EC), sulfate
350 (SO_4^{2-}), nitrate (NO_3^-), ammonium (NH_4^+), sea salt (SEAS), and fine-mode unspiciated
351 aerosols ($\text{AP}_{2.5}$)), and additional coarse PM_{10} (PMC) ~~are were~~ extracted as analysis
352 variables, ~~which are and were~~ updated ~~by using~~ the $\text{PM}_{2.5}$ and PMC observations,
353 respectively. Before ~~the calculation of~~ calculating equation (1) within the GSI, the

354 analysis variables ~~are~~were bilinearly interpolated in the horizontal direction to the
355 observation locations.

356 ~~The computation of~~Calculating background error covariance (\mathbf{B}) is generally costly and
357 difficult when a high-dimensional numerical model is used. For simplification, \mathbf{B} ~~is~~was
358 represented as a product of spatial correlation matrices and standard deviations (SDs):

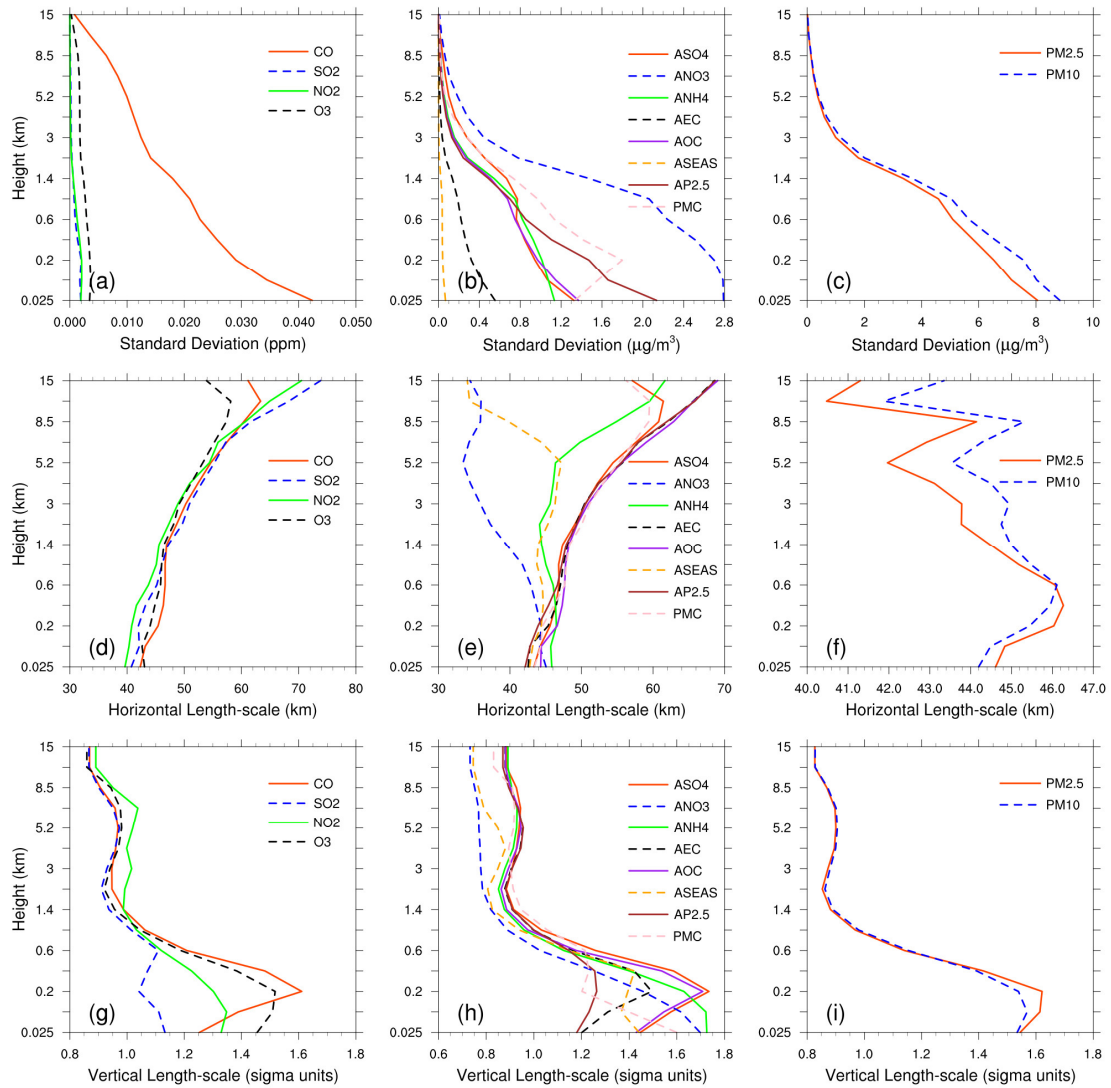
$$359 \quad \mathbf{B} = \mathbf{D}\mathbf{C}\mathbf{D}^T \quad (4)$$

$$360 \quad \mathbf{C} = \mathbf{C}_x \otimes \mathbf{C}_y \otimes \mathbf{C}_z \quad (5)$$

361 where \mathbf{D} is the background error SD matrix; \mathbf{C} is the background error correlation
362 matrix; \otimes ~~denotes~~is the Kronecker product; and \mathbf{C}_x , \mathbf{C}_y , and \mathbf{C}_z denote three one-
363 dimensional correlation submatrices in the longitude, latitude, and vertical coordinate
364 directions, respectively. \mathbf{C}_x and \mathbf{C}_y are assumed to be horizontally isotropic
365 ~~horizontally~~ such that they can be represented using a Gaussian function. The
366 correlation between any two points x_i and x_j in the horizontal direction ~~can be~~is
367 expressed as follows:

$$368 \quad c(x_i, x_j) = e^{-\frac{(x_i-x_j)^2}{2L^2}} \quad (6)$$

369 where L is the horizontal correlation scale, ~~which is~~ estimated using the proxy of the
370 background error (Figure 3). The vertical correlation matrix \mathbf{C}_z is directly estimated
371 from the model background field ~~since~~as \mathbf{C}_z is only an $n_z \times n_z$ (here, $n_z=15$)
372 matrix.



373

374 **Figure 3.** Vertical profiles of standard deviations (top, $\mu\text{g m}^{-3}$), horizontal ~~length scale~~
 375 (middle, km) and vertical ~~length scale~~ (bottom, km) length scales for CO, SO₂, NO₂,
 376 O₃, sulfate, nitrate, ammonium, EC, OC, sea salt, unspicated aerosols (AP_{2.5}), PMC,
 377 PM_{2.5} and PM₁₀.

378 To estimate these matrices, the “NMC” method ~~is-was~~ used ~~here~~ to compute **B** for each
 379 variable by taking the differences between forecasts of different lengths valid at the
 380 same time (Parrish and Derber, 1992; Rabier et al., 1998). Differences between the 24-
 381 and 12-h WRF/CMAQ forecasts of 60 pairs (two pairs ~~a-per~~ day) of analysis variables
 382 valid at either 0000 or 1200 UTC over November 2016 ~~are-were~~ used. The horizontal
 383 and vertical length scales of the correlation matrices ~~are-were~~ estimated ~~by-using~~
 384 recursive filters (Purser et al., 2003). The vertical distribution of the background error

SDs ~~is shown in Figure 3~~, which varies with height and species, is shown in Figure 3. The vertical profile of the background error SDs corresponds to the vertical concentration distribution. This means that higher concentrations tend to have larger background error SDs (e.g., CO and nitrate). These SDs exhibit a common reduction ~~with as the~~ height increases, especially at the top of the boundary layer. The horizontal correlation of the background error determines the propagation of observation information in this direction, ~~while-whereas the~~ vertical correlation determines the vertical extension of such increments. For gaseous pollutants and most individual aerosol components, the horizontal length scales ~~increas~~ed with height, ~~wher~~ea~~sh~~ile for the total particulate matter (i.e., PM_{2.5} ~~and~~ PM₁₀), the scales ~~increas~~ed with height in the boundary layer and ~~decreas~~d with height in the free troposphere. The ground-level scale generally ~~spread~~s 40 ~~–~~45 km for all control variables ~~on average~~. The vertical length scale of most species first ~~increas~~ed ~~first~~ and then ~~decreas~~ed with height, which may be related to ~~the~~ vertical mixing (Kahnert, 2008) and stack emissions at approximat~~ely~~ly about 200 m height.

2.1.4 EnKF assimilation algorithm

In EnKF, the time-dependent uncertainties of the state variables are estimated using a Monte Carlo approach through an ensemble. Uncertainty can be propagated ~~with using~~ linear or nonlinear dynamic models (flow-dependent background error covariance) by simply implementing ensemble simulations. The EnSRF algorithm introduced by Bierman (1977) and Maybeck (1979) ~~is was~~ used to constrain pollution emissions in this study. EnSRF is a deterministic EnKF that obviates the need to perturb observations, which has a higher computational efficiency and a better performance (Sun et al., 2009).

The perturbation of the prior emissions represents the uncertainty. We ~~implement~~ed additive emission adjustment methods, which ~~are were~~ calculated using the following function:-

$$\mathbf{X}_i^b = \mathbf{X}_0^b + \delta \mathbf{X}_i^b, i = 1, 2, \dots, N \quad (7)$$

where **b** ~~represents is~~ the background (prior) state, *i* is the identifier of the perturbed

413 samples, and N is the ensemble size, which was set to 40 ~~in consideration of~~ considering
414 ~~the~~ trade-off between ~~the~~ computational al cost and inversion accuracy (Figure S1). In
415 contrast to the estimation of parameters based on the augmentation of the conventional
416 state vector (e.g. concentrations) with the parameter variables, X only comprises
417 emissions in this study (similarly hereafter). δX_i^b ~~represents~~ is the randomly perturbed
418 samples ~~that are~~ added to the prior emissions X_0^b to produce ensemble samples of the
419 inputs X_i^b . δX_i^b is drawn from Gaussian distributions with a mean of zero and ~~the~~
420 standard deviation of the prior emission uncertainty in each grid. The state variables of
421 the emissions include CO, SO₂, NO_x, primary PM_{2.5} (PPM_{2.5}) and PMC. We used
422 variable localization to update the analysis, which means that the covariance among
423 different state variables was not considered, and the emission of one species was only
424 constrained only by ~~with~~ its corresponding air pollutant observation. This method has
425 been widely used in chemical data assimilation systems to avoid spurious correlations
426 among-between species- (Ma et al., 2019; Miyazaki et al., 2012b).

427 After obtaining an ensemble of state vectors (prior emissions), ensemble runs of the
428 CMAQ model ~~are-were~~ conducted to propagate ~~these~~ errors in the model with each
429 ensemble sample of state vectors. Combined with the observational vector y , the state
430 vector ~~is-was~~ updated by minimizing the analysis variance.:

$$431 \quad \bar{X}^a = \bar{X}^b + \mathbf{K}(y - \mathbf{H}\bar{X}^b) \quad (8)$$

$$432 \quad \mathbf{K} = \mathbf{P}^b \mathbf{H}^T (\mathbf{H} \mathbf{P}^b \mathbf{H}^T + \mathbf{R})^{-1} \quad (9)$$

$$433 \quad \mathbf{P}^b = \frac{1}{N-1} \sum_{i=1}^N (X_i^b - \bar{X}^b) (X_i^b - \bar{X}^b)^T \quad (10)$$

$$434 \quad \delta X_i^a = \delta X_i^b - \tilde{\mathbf{K}} \mathbf{H} \delta X_i^b \quad (11)$$

435 While employing sequential assimilation and independent observations, $\tilde{\mathbf{K}}$ is
436 calculated as follows:

$$437 \quad \tilde{\mathbf{K}} = \left(1 + \sqrt{\mathbf{R} / (\mathbf{H} \mathbf{P}^b \mathbf{H}^T + \mathbf{R})} \right)^{-1} \mathbf{K} \quad (12)$$

438 where $\bar{\mathbf{X}}^b$ ~~represents is~~ the mean of the ensemble samples; \mathbf{H} is the observation
 439 operator that maps simulated concentrations from the model space to the observation
 440 space; $\mathbf{y} - \mathbf{H}\bar{\mathbf{X}}^b$ reflects the differences between the simulated and observed
 441 concentrations; \mathbf{P}^b is the ensemble-estimated background (a priori) error covariance;
 442 $\mathbf{P}^b \mathbf{H}^T$ contains the response of the uncertainty in the simulated concentrations to the
 443 uncertainty in emissions; \mathbf{K} is the Kalman gain matrix of the ensemble mean depending
 444 on the \mathbf{P}^b and observation error covariance \mathbf{R} , representing the relative contributions
 445 to analysis; and $\tilde{\mathbf{K}}$ is the Kalman gain matrix of the ensemble perturbation, which is
 446 used to calculate emission perturbations after inversions $\delta \mathbf{X}_i^a$. The ensemble mean $\bar{\mathbf{X}}^a$
 447 of the analyzed state ~~is taken as~~ was considered the best estimate of the emissions.

448 ~~With-When~~ large volumes of site observations ~~that are recorded~~ at a much higher
 449 resolution than the model grid spacing, ~~many there would be significant~~ correlated or
 450 fully consistent model-data mismatch errors can appear in one cluster, resulting in
 451 excessive adjustments and deteriorated model performances (Houtekamer and Mitchell,
 452 2001). To reduce the horizontal observation error correlations and ~~the~~ influence of
 453 representativeness errors, a “super-observation” approach combining multiple noisy
 454 observations located within the same grid and assimilation window ~~is was~~ developed
 455 based on optimal estimation theory (Miyazaki et al., 2012a). Previous studies ~~have~~
 456 demonstrated the necessity ~~of for~~ data-thinning and dealiasing errors (Feng et al., 2020b;
 457 Zhang et al., 2009a). The super-observation y_{new} , super-observation error r_{new} , and
 458 corresponding simulation $x_{new,i}$ of the i th sample are calculated as follows:

$$459 \quad 1/r_{new}^2 = \sum_{j=1}^m 1/r_j^2 \quad (13)$$

$$460 \quad y_{new} = \sum_{j=1}^m w_j y_j / \sum_{j=1}^m w_j \quad (14)$$

$$461 \quad x_{new,i} = \sum_{j=1}^m w_j x_{ij} / \sum_{j=1}^m w_j \quad (15)$$

462 where j is the identifier of m observations within a super-observation grid; r_j is the
 463 observational error of the actual j th observation y_j ; x_{ij} ~~represents as the~~ simulated

464 concentration using the i th prior emission sample corresponding to the j th observation;
465 and $w_j = 1/r_j^2$ is the weighting factor. The super-observation error decreaseds as the
466 number of observations used within a super-observation increases. This method ~~has~~
467 ~~been~~was used in our previous inversions using surface-based (Feng et al., 2020b) and
468 satellite-based (Jiang et al., 2021) observations.

469 In this study, the DA window was set to ~~1~~one day because the model ~~need~~requires a
470 longer time to integrate the emission information into the concentration ensembles (Ma
471 et al., 2019). Due to the “super-observation” approach, only one assimilation is needed
472 in one assimilation window. In addition, ~~due to~~owing to the complexity of hourly
473 emissions, it is ~~very~~ difficult to simulate hourly concentrations that ~~can~~ match the
474 observations well. Although a longer DA window ~~could~~would allow more observations
475 to constrain the emission change of one grid, the spurious correlation signals of EnKF
476 would attenuate the observation information ~~over~~with time (Bruhwiler et al., 2005;
477 Jiang et al., 2021). Kang et al. (2012) conducted OSSEs and demonstrated that ~~due~~
478 ~~to~~owing to the ~~errors of~~ transport errors and increasedd ~~the~~ spurious correlation, a longer
479 DA window (e.g., 3 weeks) would cause the analysis system to blur ~~out the~~ essential
480 emission information ~~far~~ away from the observation. Therefore, daily mean simulations
481 and observations ~~were~~are used in the EnSRF algorithm, and daily emissions ~~were~~are
482 optimized in this system.

483 EnKF is subject to spurious correlations ~~due to~~because of the limited number of
484 ensembles when it is applied in high-dimensional atmospheric models, which can cause
485 rank deficiencies in the estimated background error covariance and filter divergence,
486 and further degrade analyses and forecasts (Wang et al., 2020). Covariance localization
487 is performed to reduce spurious correlations caused by ~~the a~~ finite ensemble size
488 (Houtekamer and Mitchell, 2001). Covariance localization preserves the meaningful
489 impact of observations on state variables within a certain distance (cutoff radius) but
490 limits the detrimental impact of observations on remote state variables. The localization

491 function of Gaspari and Cohn function (Gaspari and Cohn, 1999) is used in this system,
492 which is a piecewise continuous fifth-order polynomial approximation of a normal
493 distribution. The optimal localization scale is related to the ensemble size, assimilation
494 window, dynamic system, and lifetime of ~~a the~~ chemical species in the atmosphere. CO,
495 SO₂ and PM_{2.5} are rather stable in ~~the~~ atmosphere, with a lifetime ~~of~~ more than ~~one~~
496 day. According to the averaged ~~d~~ wind speed (3.3 m/s, Table 4) and ~~the~~ length of ~~the~~ DA
497 window, ~~their the~~ localization scales ~~of CO, SO₂ and PM_{2.5} are were~~ set to 300 km. In
498 addition, ~~the localization scales of~~ NO₂, ~~which~~ is rather reactive ~~and has, with~~ a lifetime
499 of approximately 10 hours in winter (de Foy et al., 2015), and PMC, which ~~is~~ mainly
500 from local sources ~~and has a short, its~~ residence time in the atmosphere ~~is also short due~~
501 ~~to owing to~~ the rapid deposition rate (Clements et al., 2014; Clements et al., 2016; Hinds,
502 1982). ~~Their localization scales are were~~ set to 150 ~~km~~ and 250 km, respectively.

503 2.2 Prior emissions and uncertainties

504 ~~The a~~ Anthropogenic emissions over China were ~~taken obtained~~ from the 2016 Multi-
505 resolution Emission Inventory for China (MEIC 2016) (Zheng et al., 2018), while those
506 over the other regions of East Asia were obtained from the mosaic Asian anthropogenic
507 emission inventory (MIX) (Li et al., 2017). The spatial resolutions of ~~both the~~ MEIC
508 and MIX inventories ~~were both are~~ 0.25° × 0.25°, and they are ~~both~~ downscaled to
509 match the model grid spacing of 36 km. The spatial distributions of ~~the~~ CO, SO₂, NO_x,
510 PPM_{2.5}, and PMC emissions are shown in Figure 12. The daily emission inventory,
511 which was arithmetically averaged from the combined monthly emission inventory, was
512 directly used in the EI subsystem and ~~was~~ employed as the prior emission of the first
513 DA window in the EI subsystem (Figure 1). During the simulations, ~~the~~ daily emissions
514 were further converted to hourly emissions. ~~For a All the~~ species emitted from area
515 sources, ~~we were~~ converted ~~them~~ to hourly ~~emissions~~ using ~~a the~~ same diurnal profile
516 (Figure S2), and for the point source, we assumed that there was no diurnal change.
517 MEIC 2012 was used as an alternative a priori over China to investigate the impact of
518 different prior emissions on ~~the~~ optimized emissions. The Model of Emissions of Gases
519 and Aerosols from Nature (MEGAN) (Guenther et al., 2012) was used to calculate time-

520 dependent biogenic emissions. ~~It, which~~ was ~~also~~ driven by the WRF model ~~in this~~
521 ~~study~~. Biomass burning emissions were not included because they have little impact
522 across China during the study period (Zhang et al., 2020).

523 During the inversion cycles, ~~the~~ inverted emissions of different members converge
524 ~~gradually~~ gradually, and the ensemble-estimated error covariance matrix is
525 ~~arithmetically~~ likely to be underestimated. To avoid this, considering the compensation
526 of model errors and comparable emission uncertainties from one day to the next, we
527 imposed the same uncertainty on emissions at each DA window. As mentioned above,
528 the optimized emissions of the current DA window ~~are~~ were transferred to the next DA
529 window as prior emissions. The technology-based emission inventory developed by
530 Zhang et al. (2009b), ~~basically~~ using the same method as MEIC, ~~showeds~~ that the
531 emissions of PMC and PPM_{2.5} ~~have~~ had the largest uncertainties, followed by CO, and
532 finally SO₂ and NO_x. Therefore, the uncertainties of PMC, PPM_{2.5}, CO, SO₂, and NO_x
533 in this study ~~are~~ were set ~~to~~ as 40%, 40%, 30%, 25%, and 25%, respectively. However,
534 previous studies have shown that ~~the~~ inversely estimated CO and PMC emissions ~~could~~
535 can exceed 100% higher than the bottom-up emissions (MEIC) in certain areas (Feng
536 et al., 2020b; Ma et al., 2019). Therefore, ~~a~~ According to the extent of underestimation,
537 we set an uncertainty of 100% for both the CO and PMC emissions at the beginning of
538 the three DA windows to quickly converge the emissions. ~~The~~ ~~m~~ Mean emission
539 analysis is generally minimally sensitive to the uncertainty setting in ~~our~~ the
540 assimilation cycle method (Feng et al., 2020; Gurney et al., 2004; Miyazaki et al., 2012a)
541 ~~because~~ as the inversion errors of the current window ~~could~~ can be transferred to the
542 next window for further optimization (Section 4.3).

543 **2.3 Observation data and errors**

544 Hourly averaged surface CO, SO₂, NO₂, O₃, PM_{2.5}, and PM₁₀ observations from 1504
545 national control air quality stations were assimilated into this system, which were
546 obtained from the Ministry of Ecology and Environment of the People's Republic of
547 China (<http://106.37.208.233:20035/>, last access: 25 June 2020). These sites are
548 distributed over most of central and eastern China and become denser near metropolitan

549 areas (see Figure 2). ~~Value-range and time-continuity checks were performed to~~ ensure
550 data quality. ~~Value-range checks were mainly performed to eliminate unrealistic or~~
551 ~~unrepresentative observations and. Only the~~ observations within the subjectively
552 selected threshold range were assimilated (Table 2). ~~In additionally, a~~ time-continuity
553 check was performed to eliminate gross outliers and ~~a sudden anomalies~~ using ~~the~~
554 function of $\max(|O(t) - O(t \pm 1)|) \leq f(t)$, where $O(t)$ and $O(t \pm 1)$ represent
555 observations at time t and $t \pm 1$, respectively, and $f(t) = T_a + T_b \times O_t$. ~~That This~~
556 means that ~~both the~~ concentration differences between time t and time $t+1$ and $t-1$
557 should be less than $f(t)$. ~~T_b is was~~ fixed ~~to at~~ 0.15, and the section of T_a is given in
558 Table 2, which ~~is was~~ determined empirically according to the time series change of
559 concentration at each site. ~~It should be noted that, to~~ avoid potential cross-correlations,
560 we assimilated PM_{2.5} and PMC. Additionally, in the EI subsystem, the observations
561 within each city were averaged to ~~thin-reduce~~ the data density, reduce the error
562 correlation, and increase ~~the~~ spatial representation (Houtekamer and Mitchell, 2001;
563 Houtekamer and Zhang, 2016). Finally, 336 city sites ~~are were~~ available across ~~the~~
564 mainland ~~of~~ China, in which data from 311 cities' ~~data~~ were selected for assimilation
565 and the remaining 25 were selected for independent validation (Figure 2). In the IA
566 subsystem, ~~due-owing~~ to the small horizontal correlation scale (Figure 3), ~~to-obtain~~
567 ~~more-extensive-observation-constraints,~~ all site observations were assimilated to
568 provide a good IC for the next emission inversion to obtain more extensive observation
569 constraints.

570 The observation error covariance matrix (\mathbf{R}) includes both the measurement and
571 representation errors. The measurement error ε_0 is defined as follows:

$$572 \quad \varepsilon_0 = ermax + ermin \times \Pi_0 \quad (16)$$

573 where $ermax$ is ~~the~~ base error, and Π_0 denotes the observed concentration. These
574 parameters for different species are listed in Table 2, ~~which are and were~~ determined
575 according to Chen et al. (2019), Feng et al., (2018), and Jiang et al. (2013b).

576 The representative error depends on the model resolution and ~~the~~ characteristics of the

577 observation locations, which were calculated using the equations of Elbern et al. (2007),
 578 defined as follows:

$$579 \quad \varepsilon_r = \gamma \varepsilon_0 \sqrt{\Delta l / L} \quad (17)$$

580 where γ is a tunable parameter (here, $\gamma=0.5$), Δl is the grid spacing (36 km), and L
 581 ~~indicates is~~ the radius (~~here, 3~~ km for simplification) of ~~the~~ influence area of ~~an the~~
 582 observation. The total observation error (r) ~~is was~~ defined as follows:

$$583 \quad r = \sqrt{\varepsilon_0^2 + \varepsilon_r^2} \quad (18)$$

584 **Table 2.** Parameters of quality control and measurement error

Parameter	CO mg m ⁻³	SO ₂ μg m ⁻³	NO ₂ μg m ⁻³	O ₃ μg m ⁻³	PM _{2.5} μg m ⁻³	PMC μg m ⁻³
value-range	0.1-12	1-800	1-250	1-250	1-800	1-900
time-continuity (T_a)	2.5	160	70	80	180	180
ermax	0.05	1	1	1	1.5	1.5
ermin	0.5%	0.5%	0.5%	0.5%	0.75%	0.75%

585

586 **3 Experimental design**

587 RAPAS was conducted according to the procedure and settings described in Section- 2.
 588 December is one of the months with ~~the~~ most severe air pollution, ~~while whereas~~ July
 589 is one of the least polluted months in China. Therefore, this study mainly tested the
 590 performance of the RAPAS system ~~in over~~ these two months. For December, the IA
 591 subsystem was run from 26 ~~November~~ to 31, ~~November~~ 2016, with a 6-hour interval
 592 cycling assimilation to optimize ICs (ICDA). A better IC at 0000 UTC on 1 December
 593 ~~can could~~ be obtained by a five5-day high-frequency cycling assimilation and
 594 atmospheric mixing. ~~Then~~ The EI subsystem was ~~then~~ run for December 2016 with a
 595 one1-day assimilation window to optimize emissions (EMDA). ~~In For~~ July, the system
 596 ~~also operated identically to that of in the same way as for~~ December. It ~~needs to should~~

619 be noted that ~~due to~~owing to the stronger atmospheric oxidation, the lifetime of NO₂ in
620 July ~~is~~was significantly shorter than that in December;⁵ thus,² we adopted a smaller
621 localization scale for NO₂ (80 km). Both assimilation experiments used^d the combined
622 prior emission inventories of 2016,² as described in Section~~2.2~~, and the emission base
623 year coincided^s with the research stage. An Observing Systems Simulation Experiment
624 (OSSE) was conducted to evaluate the performance of the RAPAS system, which has
625 been widely used in previous assimilation systems development (Daley, 1997). In the
626 OSSE experiment, we used the MEIC 2016 inventory as a “true” emission,⁷ and reduced
627 ~~the “true” emission~~ by 30% over ~~the~~ mainland ~~of~~ China as a prior emission. The
628 simulations were simulated using the “true” emission and sampled according to the
629 locations and times of the real observations ~~were~~ used as artificial observations. The
630 observation errors ~~are~~were the same as those in EMDA. To evaluate the IC
631 improvements from the IA subsystem, an experiment without 3DVAR (NODA) ~~is~~was
632 conducted with the same meteorological fields and physical and chemistry
633 parameterization settings as those of the ICDA. To evaluate the posterior emissions of
634 the EI subsystem, two parallel forward modelling experiments ~~are~~were performed for
635 December 2016,~~namely;~~² a control experiment (CEP) with prior (MEIC 2016)
636 emissions and a validation experiment (VEP) with posterior emissions. Both
637 experiments used^d the same IC at 0000 UTC on December 01 generated through the IA
638 subsystem. ~~Similar to the above,~~[†] The only differences between CEP and VEP ~~are~~were
639 emissions. Table 3 ~~gives a summary of~~summarizes the different emission inversion
640 experiments conducted in this study.

619 To investigate the robustness of our system, ~~8~~eight sensitivity tests (from EMS1 to
620 EMS8;⁵ see Table 3) ~~are~~were performed. These experiments ~~are~~were all based on
621 EMDA. In EMS1, rather than forward simulation~~ed~~ using the optimized emissions of
622 the previous DA window in EMDA, the ICs of each DA window were first taken from
623 the forward simulation with the prior emissions of the previous DA window,⁵ and then
624 optimized using the ~~3DVAR~~EnSRF algorithm and the observations at the
625 corresponding moment,² as mentioned in Section~~2.3~~. The objective of this experiment

626 ~~is-was~~ to investigate the advantages of the “two-step” calculation scheme in the EI
627 subsystem ~~as introduced in Sect. 2.1~~. EMS2 used~~s~~ MEIC 2012 as the original prior
628 emission in China, aiming to investigate the impact of different prior inventories on the
629 estimates of emissions. ~~The Four~~ other experiments, ~~namely~~ (EMS3–6), aimed to
630 test the impact of different prior uncertainty settings, in which, the prior uncertainties
631 ~~are-were~~ reduced by -50% and -25%, and increased by 25% and 50%, respectively.
632 EMS7 aimed~~s~~ to evaluate the impact of observation errors on emission estimates, in
633 which all ~~the~~ observation errors are magnified twice. ~~The last~~ EMS8 experiment aimed~~s~~
634 to evaluate the impact of IC optimization of the first window on emission estimates, in
635 which the ICs were taken from a ~~five~~5-day spin-up simulation. Eight forward modelling
636 experiments (VEP1, VEP2, ..., VEP8) were also performed with ~~the~~ posterior
637 emissions of EMS1 to EMS8 to evaluate their performances, ~~respectively~~.

638
639
640
641
642
643
644
645
646
647
648
649
650
651
652
653
654

655 **Table 3.** Emission inversion and sensitivity experiments conducted in this study

Exp. Type	Exp. Name	Period	IC of the first DA Window	ICs of the subsequent DA window	Emission
Assimilation	EMDA	1--31 December	0000 UTC on December 1, taken from ICDA	Forecast with posterior emissions in the previous window	MEIC 2016 for December (the first DA window), optimized emissions of the previous window (other DA windows)
	OSSE	1--31 December	The s Same as EMDA	The s Same as EMDA	The s Same as EMDA, but with a decrease of 30% for CO, SO ₂ , NO _x , PPM _{2.5} , and PMC
Sensitivity	EMS1	1--31 December	The s Same as EMDA	Forecast with prior emissions in the previous window and 3DVAR assimilation <u>Optimized using the EnSRF DA method</u>	The s Same as EMDA
	EMS2	1--31 December	The s Same as EMDA	The s Same as EMDA	The s Same as EMDA, but for EMIC 2012
	EMS3-6	1--31 December	The s Same as EMDA	The s Same as EMDA	The s Same as EMDA, but with a $\pm 25\%$ or $\pm 50\%$ of default uncertainty
	EMS7	1--31 December	The s Same as EMDA	The s Same as EMDA	The s Same as EMDA, but with a +100% of default observation errors
	EMS8	1--31 December	0000 UTC on December 1, taken from ICNO	The s Same as EMDA	The s Same as EMDA

656

657

658 4 Results

659 4.1 Evaluations

660 4.1.1 Simulated meteorological fields

661 In the RAPAS system, the inversion approach attributes all ~~the~~ biases between the
662 simulated and observed concentrations to ~~the~~ emissions. ~~The m~~ Meteorological fields
663 dominate the physical and chemical processes of ~~the~~ air pollutants in the atmosphere,
664 and thus their simulation accuracy would significantly affect the estimates of emissions
665 in this study. To quantitatively evaluate the performance of the WRF simulations, the
666 mean bias (BIAS), root mean square error (RMSE), and correlation coefficient (CORR)
667 were calculated against the surface meteorological observations measured at 400
668 stations and the planetary boundary layer height (PBLH) was calculated using the
669 sounding data at 92 sites. ~~The s~~ Surface observations were obtained from the National
670 Climate Data Center (~~NCDC~~) integrated surface database
671 (<http://www.ncdc.noaa.gov/oa/ncdc.html>, last access: 25 October 2021); and ~~the~~
672 sounding data were obtained from the website of the University of Wyoming
673 (<http://weather.uwyo.edu/upperair/sounding.html>, last access: 10 March 2022). The
674 sounding data ~~are in~~ had a 12 hours interval. The observed PBLH ~~were~~ was calculated
675 using ~~the~~ sound data ~~through~~ via the bulk Richardson number method (Richardson et
676 al., 2013). The spatial distribution of ~~the~~ meteorological stations is shown in Figure 2.
677 The simulated temperature at 2 m (T2), relative humidity at 2 m (RH2), wind speed at
678 10 m (WS10), and PBLH from 26 November to 31 December 2016 ~~are~~ were evaluated
679 against the observations. Table 4 summarizes the statistical results of the evaluations of
680 the simulated meteorological parameters. Overall, ~~the~~ T2, RH2 and PBLH ~~are~~ were
681 slightly underestimated, with biases of -0.1 °C, -3.8%, and -41.1 m, respectively. ~~The~~
682 CORRs ~~are~~ were approximately 0.98 for T2, 0.94 for RH2, and 0.90 for PBLH, showing
683 good consistency between the observations and simulations. ~~The~~ WS10 ~~is~~ was
684 overestimated, with a bias of 0.7 m/s and an RMSE of 0.8 m/s, but ~~is~~ were better than
685 the simulations from many ~~other~~ previous studies (Chen et al., 2016; Jiang et al., 2012a;

Jiang et al., 2012b). Therefore, ~~the~~ WRF can generally reproduce ~~the~~ meteorological conditions sufficiently in terms of their temporal variation and magnitude over China, which is adequate for our inversion estimation.

Table 4. Statistics comparing the simulated and observed 10-m wind speed (WS10), 2-m temperature (T2), and 2-m relative humidity (RH2), and planetary boundary layer height (PBLH).

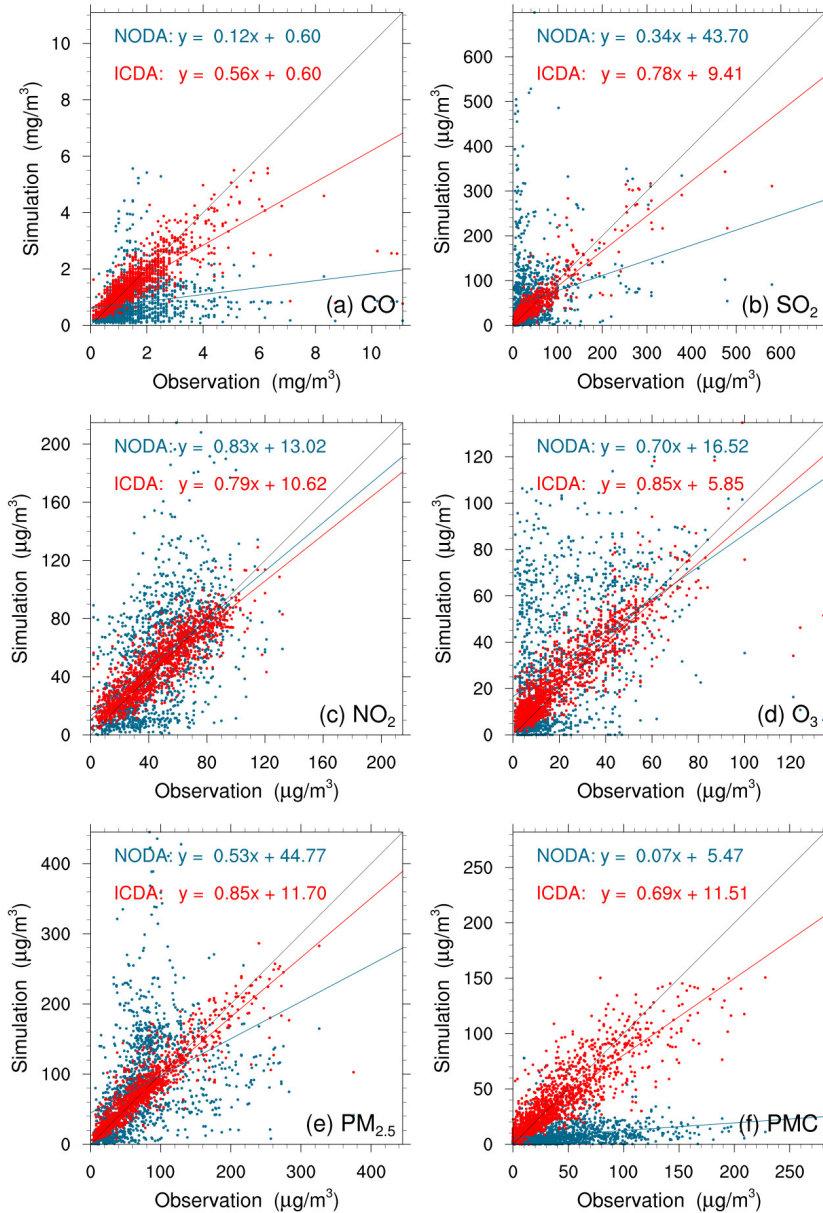
Variable Met.	No. of sites	Mean Obs.	Mean Sim.	BIAS	RMSE	CORR
WS10 (m/s)	400	2.6	3.3	0.7	0.8	0.72
T2 (°C)	400	2.9	2.8	-0.1	0.7	0.98
RH2 (%)	400	66.3	62.6	-3.8	5.2	0.94
PBLH (m)	92	267.5	226.4	-41.1	50.4	0.90

* BIAS, mean bias; RMSE, root mean square error; CORR, correlation coefficient

4.1.2 Initial ~~fields~~ conditions

Figure 4 shows ~~the-an~~ evaluations of the analyzed concentrations of the ~~6-six~~ species against surface observations. For comparison, the evaluations of the simulations without 3DVAR (NODA) are also shown in Figure 4. The simulations of the NODA experiment (red dots) are scattered on both sides of ~~a-the~~ central line, as large systematic biases remain across many measurement sites. Conversely, the ICDA experiment (blue dots) showed ~~aws~~ much better agreement with ~~the~~ observations than those from NODA. The statistics show that there are large systematic biases in the NODA simulations, with large RMSEs and small CORRs for all species, ~~especially-particularly~~ for CO and PMC. After the assimilation of surface observations, the RMSE of CO decreased~~s~~ to 0.7 mg m⁻³, and those of SO₂, NO₂, O₃, PM_{2.5}, and PMC decrease to 22.0, 12.0, 9.6, 20.5, and 19.6 μg m⁻³, respectively, with respective reductions ~~rates~~ of 50.0%, 73.1%, 61.0%, 64.7%, 69.5%, and 60.8% compared to ~~the-onesthose~~ of the NODA (Table 5). The CORRs of ICDA increased~~d~~ by 290.0%, 291.3%, 55.4%, 87.2%, 130.0%, and 214.8% to 0.78, 0.90, 0.87, 0.88, 0.92, and 0.85, respectively. These statistics indicate ~~that~~ the

708 ICs of the ground level improved ~~have been~~ significantly ~~improved~~. However, ~~due~~
 709 owing to the lack of observations, we still do not know the simulation bias in the upper-
 710 middle boundary layer. Although concentrations at high altitudes can be constrained by
 711 ground-based observations through vertical correlations, the effect is limited; therefore,
 712 ~~so~~ the bias ~~is still~~ remains non-negligible.



713
 714 **Figure 4.** Scatter plots of simulated versus observed (a) CO, (b) SO₂, (c) NO₂, (d) O₃,
 715 (e) PM_{2.5}, and (f) PMC mass concentrations at 0000 UTC on December 1 initializations
 716 from the background (red) and analysis (blue) fields.

Table 5. Comparisons of the surface CO, SO₂, NO₂, O₃, PM_{2.5} and PMC mass concentrations from the control and assimilation experiment against observations aggregated over all analysis times. CO unit: mg m⁻³; others units: μg m⁻³.

Species	Exp. Name	Mean Obs.	Mean Sim.	BIAS	RMSE	CORR
CO	NODA	1.5	0.8	-0.7	1.4	0.20
	ICDA		1.5	-0.1	0.7	0.78
SO ₂	NODA	36.3	56.0	19.7	81.7	0.23
	ICDA		37.8	1.5	22.0	0.90
NO ₂	NODA	45.8	51.1	5.3	30.8	0.56
	ICDA		47.0	1.1	12.0	0.87
O ₃	NODA	20.5	30.8	10.4	27.2	0.47
	ICDA		23.3	2.8	9.6	0.88
PM _{2.5}	NODA	70.9	82.2	11.3	67.3	0.40
	ICDA		71.8	0.9	20.5	0.92
PMC	NODA	43.5	8.5	-35.0	50.0	0.27
	ICDA		41.6	-1.9	19.6	0.85

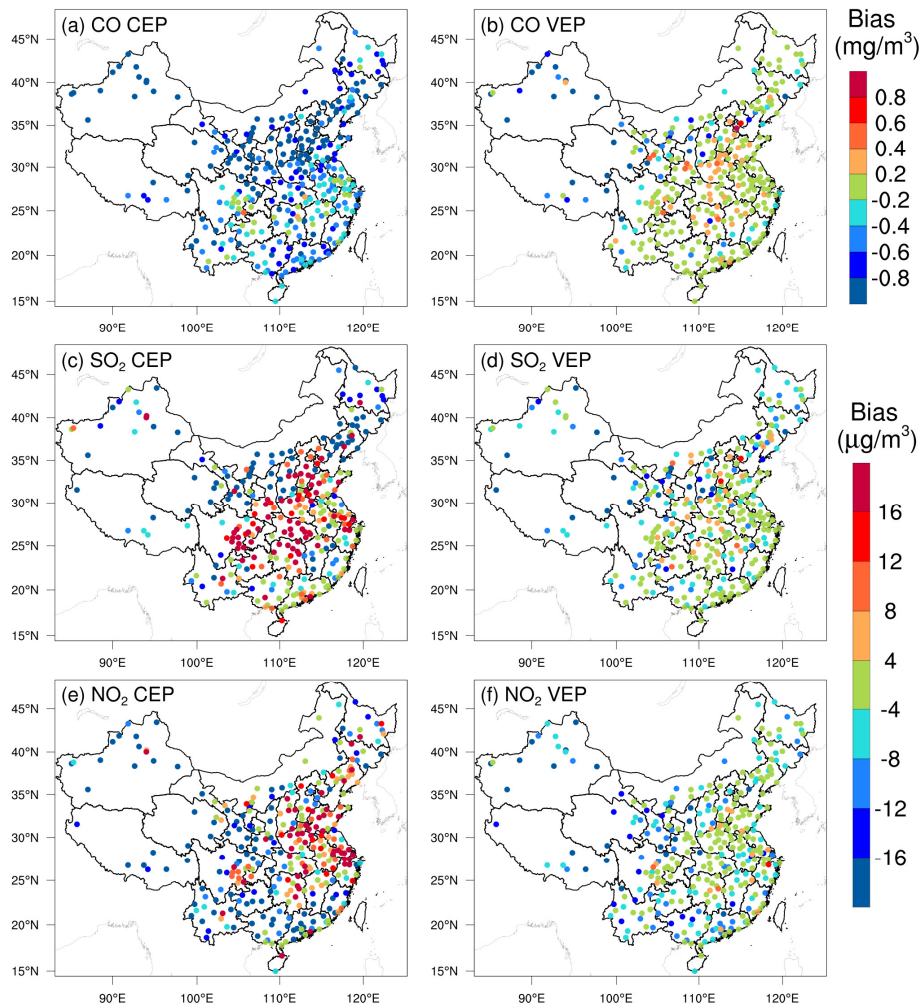
* BIAS, mean bias; RMSE, root mean square error; CORR, correlation coefficient

4.1.3 Posterior emissions

Due-Owing to the mismatched spatial scales, it is difficult to directly evaluate the optimized emissions against observations. Generally, we indirectly validated ~~them-the~~ optimized emissions by comparing the forward simulated concentrations using the posterior emissions against atmospheric measurements (e.g., Jiang et al.₁ (2014)_; Jin et al.₂ (2018)_; ~~and~~ Peters et al.₂ (2007)). Figure 5 shows the spatial distributions of the mean biases between the ~~simulated~~-gaseous pollutants simulated using prior and posterior emissions and assimilated observations. In the CEPs, for each species, the distribution of biases ~~is-was~~ similar to the increments in background fields constrained through 3DVAR₂ as shown in Figure S3. For example, almost all sites ~~have-had~~ large negative biases for CO, while for SO₂ and NO₂, positive biases ~~are-were~~ mainly distributed over the North China Plain (NCP), Yangtze River Delta (YRD), Sichuan Basin (SCB)₂ and Central China₅, and negative biases ~~are-were distributed~~ over ~~the rest~~

734 ~~of the remaining~~ areas. After constraining with observations, the biases of all ~~the 3~~three
735 gaseous air pollutants ~~are were~~ significantly reduced ~~in at~~ most sites. For CO, the biases
736 at 62% of the sites decreased to absolute values less than 0.2 mg m^{-3} ; and for SO₂ and
737 NO₂, the biases at 52% and 47% of the sites were within $\pm 4 \text{ } \mu\text{g m}^{-3}$. However, large
738 negative biases ~~are were~~ still observed in ~~part of~~ western Chinas, indicating that the
739 uncertainties of the posterior emissions are still large in western China, which may be
740 attributed to the large biases in prior emissions and ~~to~~ the relatively limited observations.
741 Overall, the statistics show that there are different levels of improvements at ~~92%, 85%~~
742 ~~and 85% of the total~~ 311 assimilation sites of 92%, 85%, and 85% for CO, SO₂, and
743 NO₂, respectively. The small ~~amount~~number of sites with worse performance may be
744 related to ~~the~~ over-adjusted emissions by EI or contradictory adjustments caused by
745 opposite biases in adjacent areas.

746 Table 6 lists the statistical results of the evaluations averaged over the whole mainland
747 of China. For CO, the mean bias ~~is was~~ -0.8 mg m^{-3} with the prior emissions, while it
748 substantially reduceds to -0.1 mg m^{-3} (~~with a~~ reduction rate of 89.6%) when simulating
749 with the posterior emissions. Additionally, the RMSE ~~decreases~~decreased by 48.1%
750 from 1.08 to 0.56 mg m^{-3} , and the CORR ~~increases~~increased by 76.1% from 0.46 to
751 0.81. For SO₂ and NO₂, the regional mean biases slightly increasedd as the
752 positive/negative biases among different sites might be offset. However, the RMSEs
753 decreasedd to 17.7 and $12.3 \text{ } \mu\text{g m}^{-3}$, respectively, which ~~are were~~ 58.3% and 50.8% lower
754 than those of CEPs, and the CORRs increasedd by 125.6% and 35.4%, both reaching up
755 to 0.88, indicating that EI ~~has~~ significantly improved the NO_x and SO₂ emission
756 estimates.

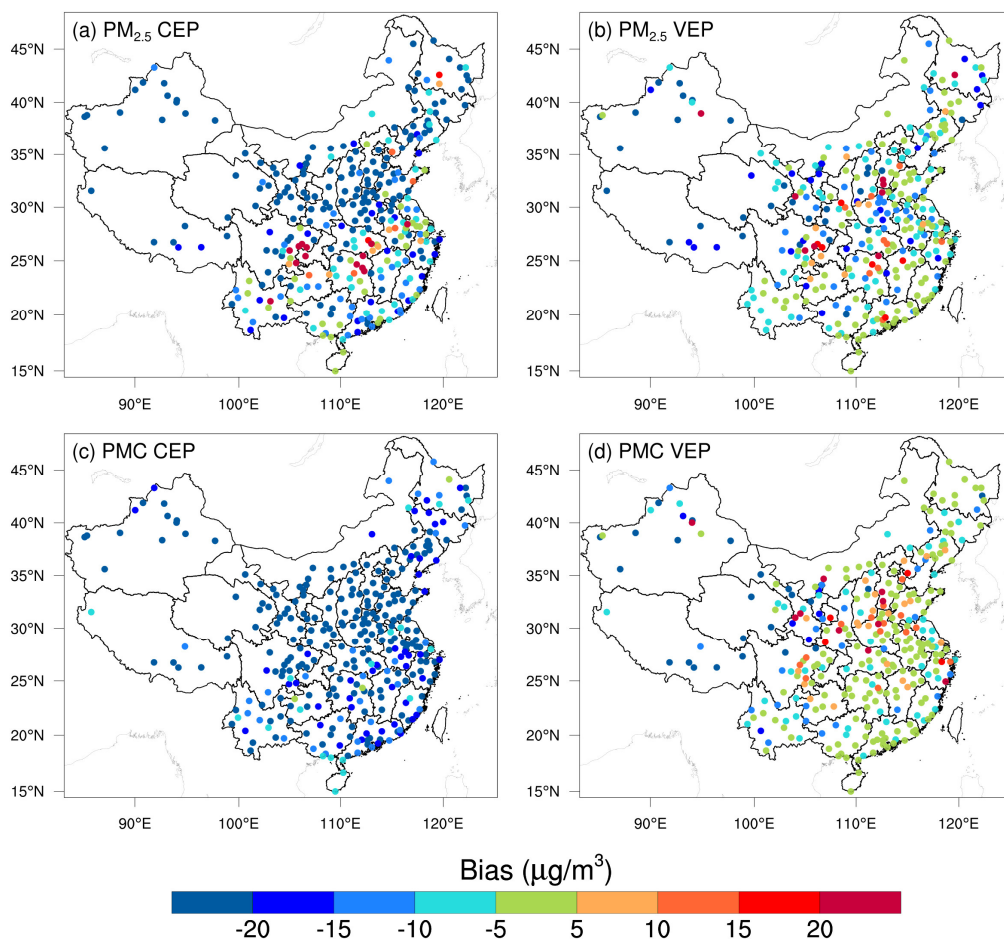


757

758 **Figure 5.** Spatial distribution of the BIAS of the simulated (a, b) CO, (c, d) SO₂ and
 759 (e, f) NO₂ with prior (left, CEP) and posterior (right, VEP) emissions. CO unit: mg m⁻³;
 760 SO₂ and NO₂ units: µg m⁻³.

761 Figure 6 shows the spatial distributions of the mean biases of simulated PM_{2.5} and PMC
 762 evaluated against ~~the~~ assimilated observations. Similarly, the CEP simulations ~~do~~ did
 763 not perform well. There ~~are~~ were widespread underestimations across the country, with
 764 mean biases of -24.0 and -32.4 µg m⁻³. After data assimilation, the performance of the
 765 VEP simulations ~~is~~ significantly improved. The biases decreased d by 72.1% and 90.4%
 766 to -6.7 and -3.1 µg m⁻³, the RMSEs decreased d by 41.2% and 40.7% to 29.6 and 24.6 µg
 767 m⁻³, and the CORRs increased d by 35.9% and 176.0% to 0.87 and 0.69 for PM_{2.5} and
 768 PMC, respectively. Overall, 89.6% and 97.2% of the assimilation sites ~~are~~ were

769 improved for PM_{2.5} and PMC, respectively. However, compared with the results ~~of~~for
 770 the ~~3~~three gaseous pollutants, there ~~are~~were sites with large biases scattered throughout
 771 the ~~whole~~entire domain. ~~Besides~~In addition to the potential over-adjusted or
 772 contradictory adjustments of emissions as in the ~~3~~three gas species, ~~It~~the sites with
 773 large biases may ~~also~~be related to the complex precursors and complex homogeneous
 774 and heterogeneous chemical reactions and transformation processes of secondary PM_{2.5},
 775 and the fact that we ~~do~~did not simulate the time variation of dust blowing caused by
 776 wind speed for PMC ~~due~~owing to the lack of land cover data that is compatible with
 777 the CMAQ dust module and agricultural activityies data to identify dust source regions.



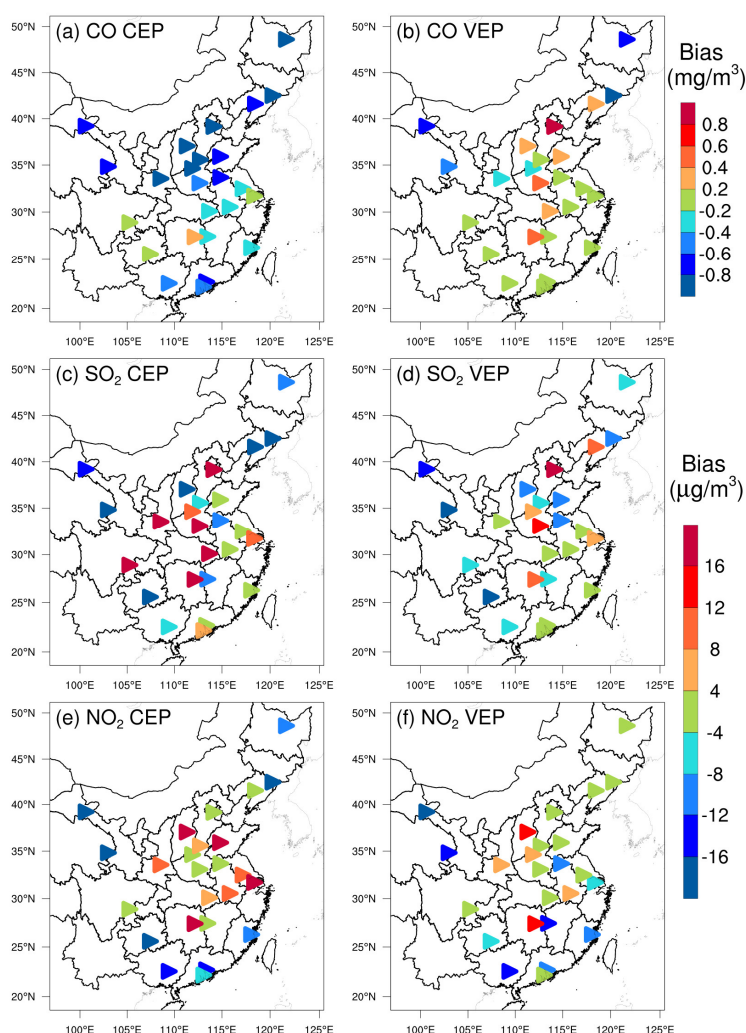
778

779

Figure 6. Same as in Figure 5 but for PM_{2.5} and PMC.

780 Figures 7 and Figure 8 show the spatial distributions of the biases calculated against the
 781 independent observations for the ~~5~~five species. With posterior emissions, the

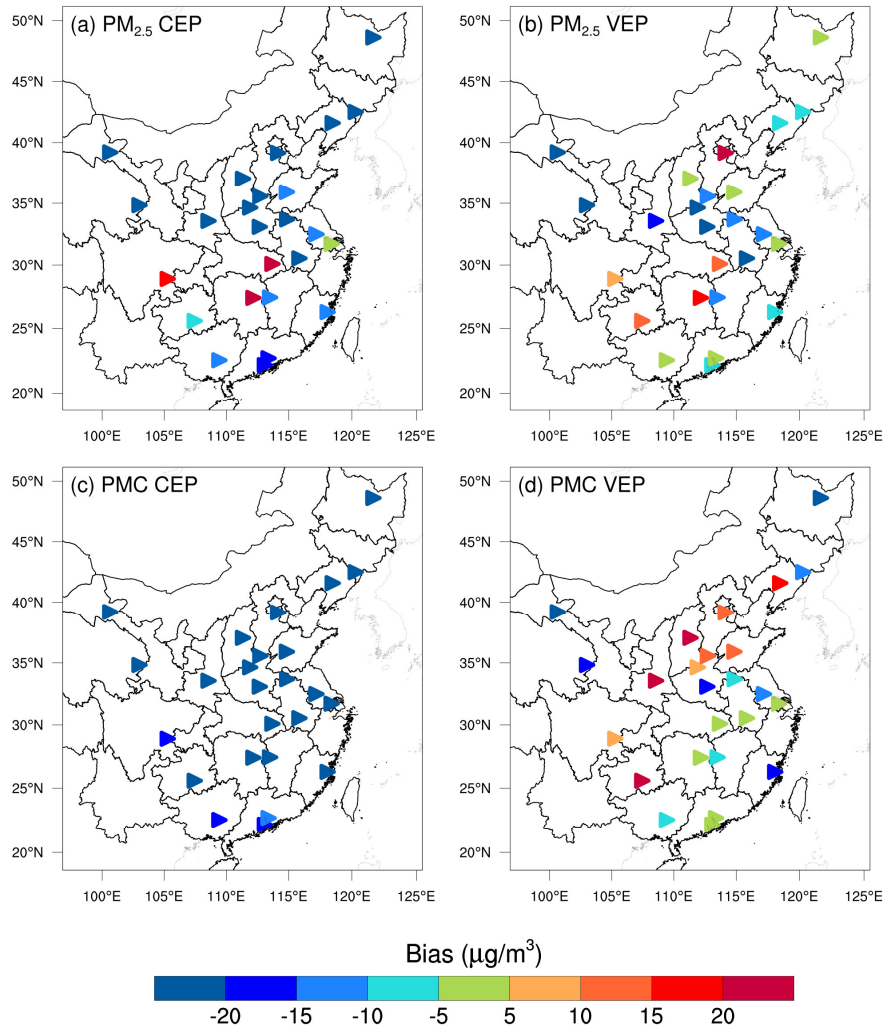
782 decreasing ratios of RMSEs ranged d from 26.7% ~~to~~ 42.0%, and the CORRs increased d
 783 by 13.7 ~~to~~ 59.0% to 0.62 ~~to~~ 0.87. Overall, the biases at the independent sites are similar
 784 or slightly worse than those at the assimilated sites, which is reasonable since as the
 785 closer the independent sites are to the assimilated site ~~the independent sites are~~, the
 786 more constraints of observation information can be obtained, and the more significant
 787 the improvements in the optimized state variables of the model ~~are more significant~~.
 788 For example, generally, the transmission distance of NO₂ is relatively short, and remote
 789 cities with small emission correlations to the cities with assimilated observations are
 790 relatively less constrained, resulting in only a 26.7% decrease in the RMSE.



791

792

Figure 7. As in Figure 5 but for the independent validation.



793

794

Figure 8. As in Figure 6 but for the independent validation.

795 Comparing our results with those of the previous studies, Tang et al. (2013)
 796 conducted inversion of inverted CO emissions over Beijing and the surrounding areas,
 797 and obtained comparable the improvements (Table 6) in the RMSE (37–48% vs. 30–
 798 51%) and the CORR (both studies ~ 0.81) are comparable; however, but the biases here
 799 could decrease we decreased the biases by 90–97%, which is much greater than their
 800 48–64% reductions. Additionally, Chen et al. (2019) showed that the RMSE of
 801 simulated SO₂ with updated SO₂ emissions decreased by 4.2–52.2% for different
 802 regions, and the CORR only increased to 0.69 at most. These improvements is are
 803 relatively smaller than our results those obtained in this study, which may be due to the
 804 insufficient adjustment of emissions caused by the underestimated ensemble spread

805 through the inflation method. The better performance in this study may be related to
 806 our inversion process, ~~which causes that makes~~ the optimized emissions of the current
 807 DA window ~~to~~ propagate to the next DA window for further correction.

808 **Table 6.** Statistics comparing the pollution concentrations from the simulations with
 809 prior (CEP) and posterior (VEP) emissions against assimilated and independent
 810 observations, respectively. CO unit: mg m⁻³; others units: µg m⁻³.

Species	Mean Obs.	Mean Sim.		BIAS		RMSE		CORR	
		CEP	VEP	CEP	VEP	CEP	VEP	CEP	VEP
Against assimilated observations									
CO	1.43	0.66	1.36	-0.77	-0.08	1.08	0.56	0.46	0.81
SO ₂	32.5	34.4	28.4	1.9	-4.1	42.4	17.7	0.39	0.88
NO ₂	43.8	40.8	39.0	-2.9	-4.8	25.0	12.3	0.65	0.88
PM _{2.5}	77.0	53.1	70.3	-24.0	-6.7	50.3	29.6	0.64	0.87
PMC	40.5	8.1	37.5	-32.4	-3.1	41.5	24.6	0.25	0.69
Against independent observations									
CO	1.54	0.79	1.52	-0.75	-0.02	1.15	0.72	0.59	0.82
SO ₂	40.6	39.2	37.3	-1.3	-3.2	44.3	27.2	0.57	0.87
NO ₂	50.2	50.0	47.5	-0.3	-2.7	21.7	15.9	0.73	0.83
PM _{2.5}	91.5	64.6	84.1	-26.9	-7.4	64.1	37.2	0.62	0.87
PMC	42.0	9.2	40.4	-32.8	-1.6	39.3	26.6	0.39	0.62

811 * BIAS, mean bias; RMSE, root mean square error; CORR, correlation coefficient

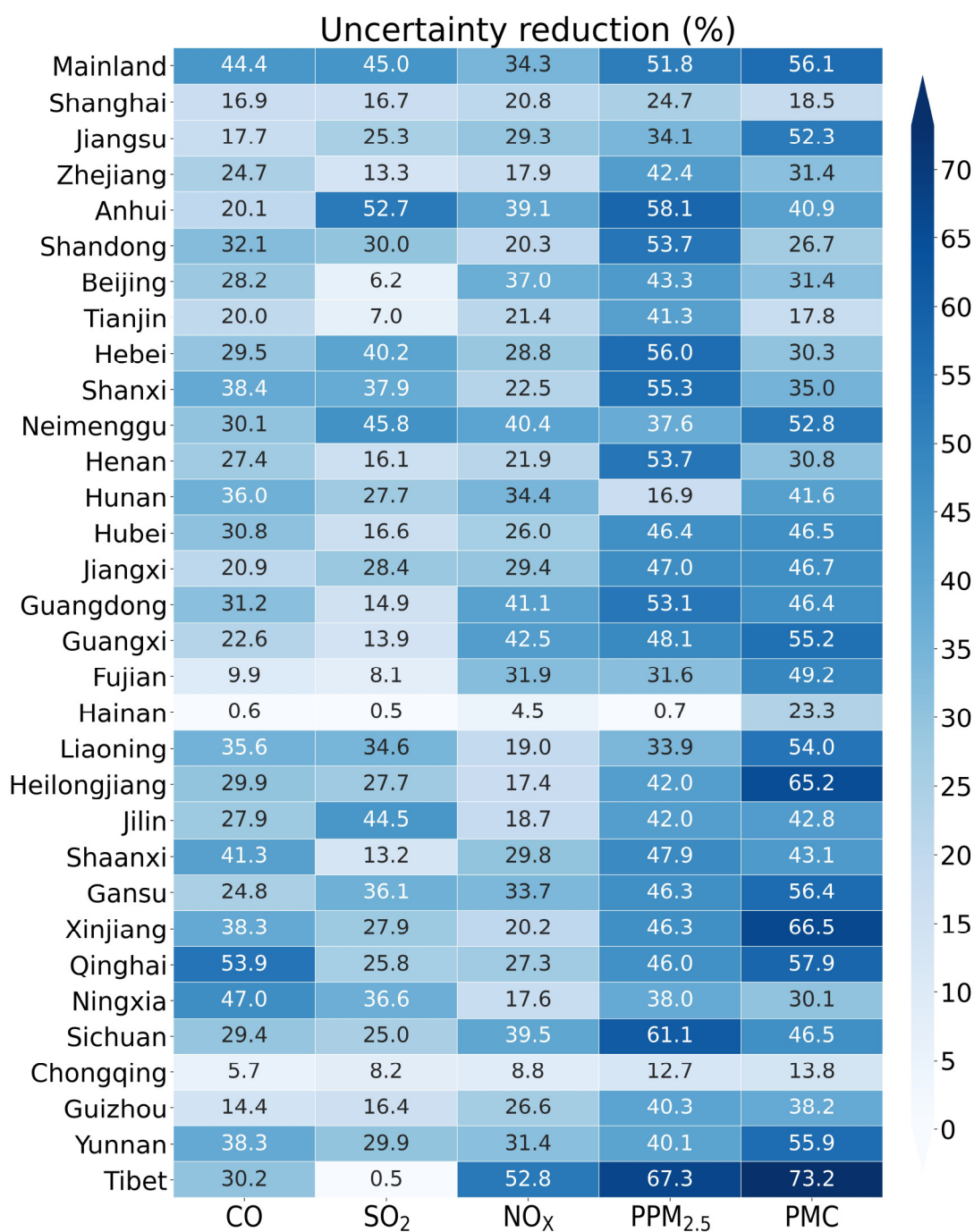
812 4.1.4 Uncertainty reduction

813 The uncertainty reduction rate (UR) is ~~another-an~~ important quantity to evaluate the
 814 performance of RAPAS and the effectiveness of ~~in situ~~ observations ~~in this~~
 815 ~~system~~ (Chevallier et al., 2007; Jiang et al., 2021; Takagi et al., 2011). Following Jiang
 816 et al. (2021), the UR ~~is-was~~ calculated as

$$817 \quad UR = \left(1 - \frac{\sigma_{posterior}}{\sigma_{prior}}\right) \times 100 \quad (19)$$

818 where $\sigma_{posterior}$ and σ_{prior} are the posterior and prior uncertainties, respectively,
 819 ~~which were~~ calculated using the standard deviations of the prior and posterior
 820 perturbations (Text S23). Figure 9 shows the URs averaged in each province and ~~the~~
 821 ~~whole~~ mainland China. ~~The~~ URs ~~varied~~ with species as they are closely related to the

822 magnitude settings of prior uncertainties (Jiang et al., 2021). The URs of PPM_{2.5} and
823 PMC were the most effective while the UR of NO_x emissions was the lowest.~~and among~~
824 ~~the 5 species of emissions, the uncertainties of the PPM_{2.5} and PMC are greatly reduced,~~
825 ~~while the UR of NO_x emission is lowest, that is because the URs are closely related to~~
826 ~~the magnitude settings of prior uncertainties (Jiang et al., 2021).~~ For ~~the whole~~-mainland
827 China overall, ~~the~~ uncertainties ~~are~~ were reduced by 44.4%, 45.0%, 34.3%, 51.8%, and
828 56.1% for CO, SO₂, NO_x, PPM_{2.5}, and PMC, respectively. For one species, ~~it~~ URs ~~also~~
829 ~~varied~~s across provinces. ~~The~~ URs are usually related to observation coverage, which
830 means that the more observation constraints there are, the more ~~the~~ URs decrease.
831 Additionally, ~~the~~ URs may also be related to emission distributions. Generally, ~~the~~ URs
832 ~~are~~ were more significant in the provinces where ~~the~~ observations and emissions ~~are~~
833 were both relatively concentrated (e.g., Tibet), while they ~~are~~ were much lower ~~in~~ where
834 the emissions ~~are~~ were scattered or relatively uniform, but the observations ~~are~~ were
835 only in large cities, even though if there ~~are~~ were many more observations than in
836 other provinces.



837

838 **Figure 9.** Time-averaged posterior emission uncertainty reduction (%) indicated by the
 839 standard deviation reduction of total emissions per province calculated by prior and
 840 posterior ensembles.

841 **4.1.5 Evaluation using chi-squared statistics**

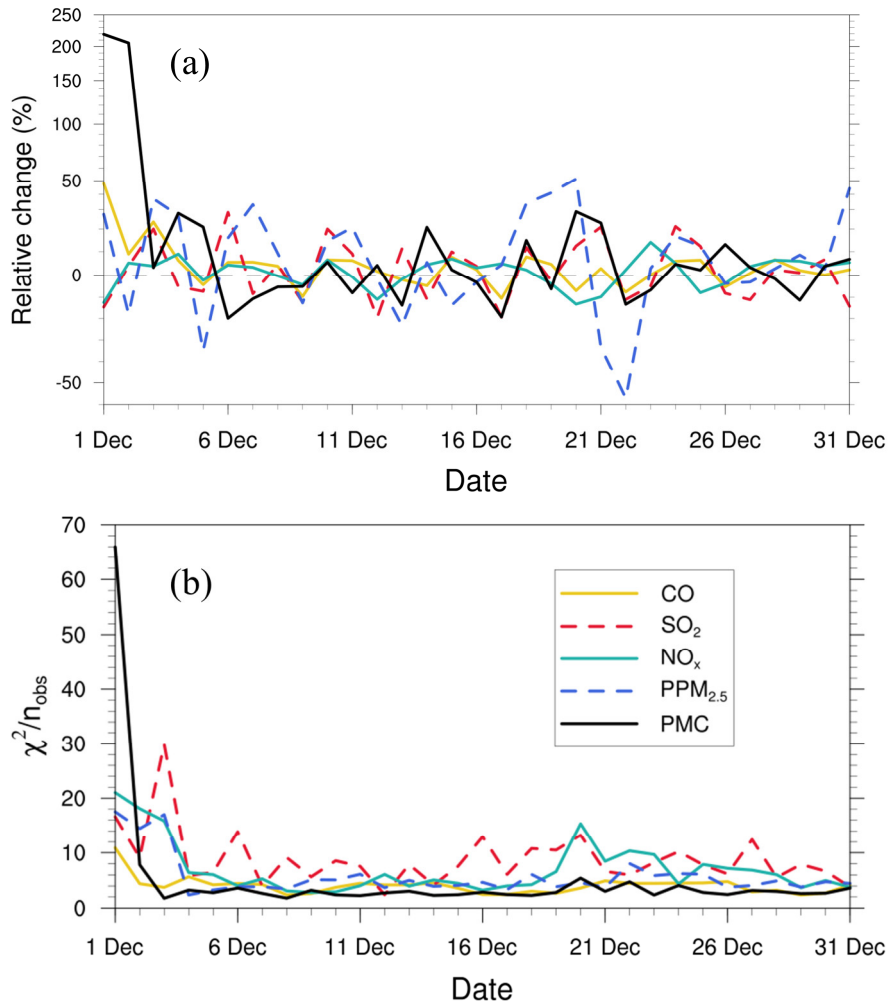
842 To diagnose the performance of the EnKF analysis, ~~the~~ chi-squared (χ^2) statistics ~~was~~
 843 were calculated, which ~~is-are~~ generally used to test whether the prior ensemble mean

844 RMSE with respect to the observations is consistent with the prior “total spread”
845 (square root of the sum of ensemble variance and observation error variance).
846 Following Zhang et al. (2015), for the t th window, χ^2 is defined as:

$$847 \quad \chi_t^2 = (\mathbf{y} - \mathbf{H}\bar{\mathbf{X}}^b)^T (\mathbf{H}\mathbf{P}^b\mathbf{H}^T + \mathbf{R})^{-1} (\mathbf{y} - \mathbf{H}\bar{\mathbf{X}}^b) \quad (20)$$

848 Figure 10 shows the time series of the relative changes between the prior and posterior
849 emissions and the χ^2 statistics. There ~~are~~were relatively large adjustments ~~of~~in
850 emissions in the first three windows, especially for the PMC. ~~Subsequently~~After that,
851 ~~the optimality of~~ the five species reacheds a more optimal state with successive
852 emission inversion cycles. The χ^2 statistics ~~shows~~showed a similar variation
853 characteristics withas the daily changes in ~~the~~ emissions. The χ^2 value ~~is~~was slightly
854 greater than 1, indicating that the uncertainties from the error covariance statistics ~~do~~
855 did not fully account for the error in the ensemble simulations. A similar result was
856 reported by ~~situation also appeared in~~ Chen et al. (2019). Further investigations should
857 be conducted to generate larger spreads by accounting for the influence of model errors.
858 ~~Since~~As we imposed the same uncertainty of prior emissionss at each DA window to
859 partially compensate for the influence of model errors, χ^2 statistics showed small
860 fluctuations, indicating that the system ~~updates~~updated emissions consistently and
861 stably.

862

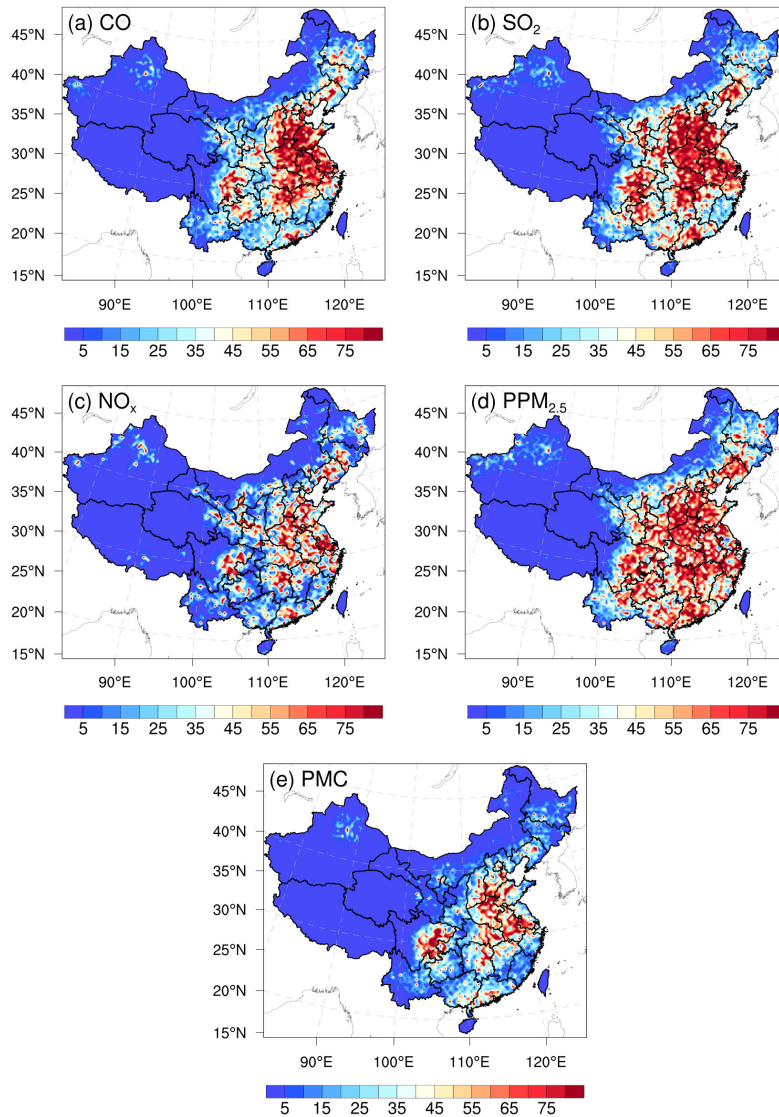


863

864 **Figure 10.** Relative changes (a) in ~~a-posteriori~~ ~~posterior~~ emission estimates of CO, SO₂,
 865 NO_x, PPM_{2.5} and PMC₅ and χ^2 statistics (b) of these state vectors in each window.

866 4.1.6 Evaluation using OSSE

867 Figure 11 shows the spatial distribution of the error reduction in the posterior emissions
 868 of the five species. ~~It can be found that a~~ After inversion, in most areas, the emission
 869 errors ~~can be were~~ reduced by more than 80%, especially in the central and eastern
 870 regions with dense observation sites, while in remote areas far away from cities, due to
 871 the sparse observation sites, the emission errors ~~are were~~ still not well adjusted. Overall,
 872 the error reduction rates of CO, SO₂, NO_x, PPM_{2.5}, and PMC ~~are were~~ 78.4%, 86.1%,
 873 78.8%, 77.6%, and 72.0%, respectively, indicating that with the ~~ground-in situ~~ ~~in situ~~
 874 observations in China, RAPAS can significantly reduce emission errors ~~and~~, thus ~~has~~
 875 ~~showed~~ good performance in emission estimates.



876

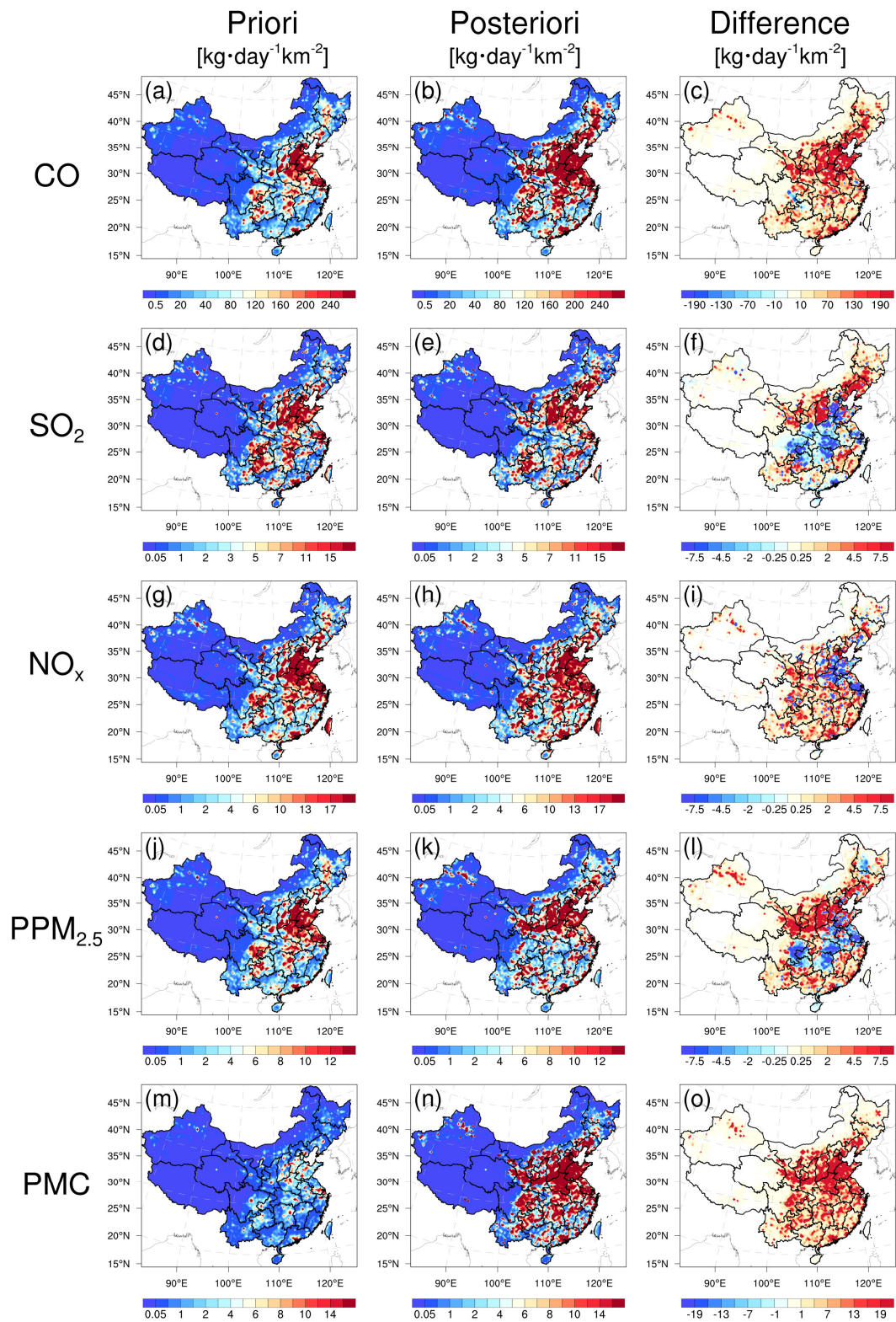
877 **Figure 11** Spatial distribution of the error reduction (%) of posterior emissions in the
 878 OSSE.

879 4.2 Inverted emissions

880 Figure 12 shows the spatial distribution of ~~the~~temporally averaged prior and posterior
 881 emissions and their differences ~~of their~~ emissions in December 2016. It should be noted
 882 that ~~the~~emissions outside China were masked; ~~assince~~ the observation sites ~~are all~~
 883 ~~within~~were limited to China in this study, there ~~is~~was little-a slight change in the
 884 emissions outside China. Higher emissions ~~are~~were mainly concentrated in central and
 885 eastern China, especially in the NCP, YRD, and PRD, and lower emissions occurred
 886 across Northwest and Southern China. Compared with the prior emissions, posterior

887 CO emissions ~~are-were~~ considerably increased across most areas of mainland China,
888 especially in northern China, with an overall increase of 129%. ~~A n~~Notable
889 underestimation of ~~the~~ prior emissions ~~is-was~~ also confirmed by ~~previous~~ inversion
890 estimations (Feng et al., 2020b; Tang et al., 2013; Wu et al., 2020) and model
891 evaluations (Kong et al., 2019b) ~~in previous studies~~. For SO₂, the emissions ~~increases~~
892 ~~increased~~ mainly ~~occur~~ in Northeast China, Shanxi, Ningxia, Gansu, Fujian, Jiangxi,
893 and Yunnan provinces. In SCB, Central China, YRD, and part of ~~the~~ NCP, ~~the~~ emissions
894 ~~are-were~~ significantly reduced. ~~For The~~ national total, ~~the~~ SO₂ emissions ~~is~~ increased
895 by 20%. For NO_x, although the increment of national total emissions ~~is-was~~ small
896 (~~approximately only about~~ 5%), ~~there were~~ large deviations ~~still exist on regional scale~~.
897 ~~Obviously, t~~The emissions in ~~the~~ NCP and YRD ~~are-were~~ reduced, ~~while-whereas in~~
898 ~~the other regions~~, the emissions ~~of in~~ most cities ~~in other regions are~~ increased. The
899 changes in ~~the emission of~~ PPM_{2.5} ~~emission are were~~ similar to ~~those of~~ SO₂. Compared
900 with the prior emissions, the posterior PPM_{2.5} emissions ~~are~~ decreased over central
901 China, SCB, and YRD, ~~while-whereas the ones those~~ in southern and northern China ~~are~~
902 increased, especially in Shanxi, Shaanxi, Gansu, and southern Hebei provinces. Overall,
903 the relative increase ~~is-was~~ 95%. For PMC, the posterior emissions ~~are-were~~ increased
904 over ~~the whole all of~~ mainland China, with national mean relative increase exceeding
905 1000%. Larger emission increments mainly ~~occurred~~ in ~~the~~ areas ~~where have with~~
906 significant anthropogenic emissions of CO and PPM_{2.5}, indicating that the large
907 underestimations of PMC emissions in the prior inventory may be mainly attributed to
908 the underestimations of anthropogenic activities. ~~In addition, t~~The absence of natural
909 dust is another reason, as the wind-blown dust scheme was not applied in this study.
910 Overall, PM₁₀ emissions (PPM_{2.5}+PMC) increased by 318%. If we assume that all the
911 increments in PM₁₀ emissions ~~is all are~~ from natural dust, that means the contribution
912 of natural dust ~~accounts accounted~~ for 75% of total PM₁₀ emissions, which is consistent
913 with the source apportionment of PM₁₀ of 75% in Changsha in Central China (Li et al.,
914 2010). Large PMC emission increments ~~are-were~~ also ~~found reported by in~~ Ma et al.
915 (2019).

916 Detailed estimations_s of posterior emissions and relative changes compared to prior
917 emissions in each province and ~~the whole~~ mainland China ~~is~~ are given in Table S1. The
918 evaluation results for July showed_{ed} that the emission uncertainty ~~can~~ could still be
919 significantly reduced_; and the performance of the system in July ~~is~~ was comparable to
920 that in December (Table S2). Additionally, the seasonal variation ~~of~~ in emissions ~~can~~
921 ~~be~~ was well reflected (Figures S4 and S5), which means that our system ~~can~~ performed
922 well at different times of the year. Note that the differences, excluding PMC, between
923 the prior and posterior emissions mainly reflect the deficiencies of the prior emissions
924 ~~because~~ as the times of the prior emissions and ~~the~~ observations ~~are~~ completely ~~were~~
925 consistent in this study.



926

927 **Figure 12.** Spatial distribution of the time-averaged prior emissions (left column, MEIC

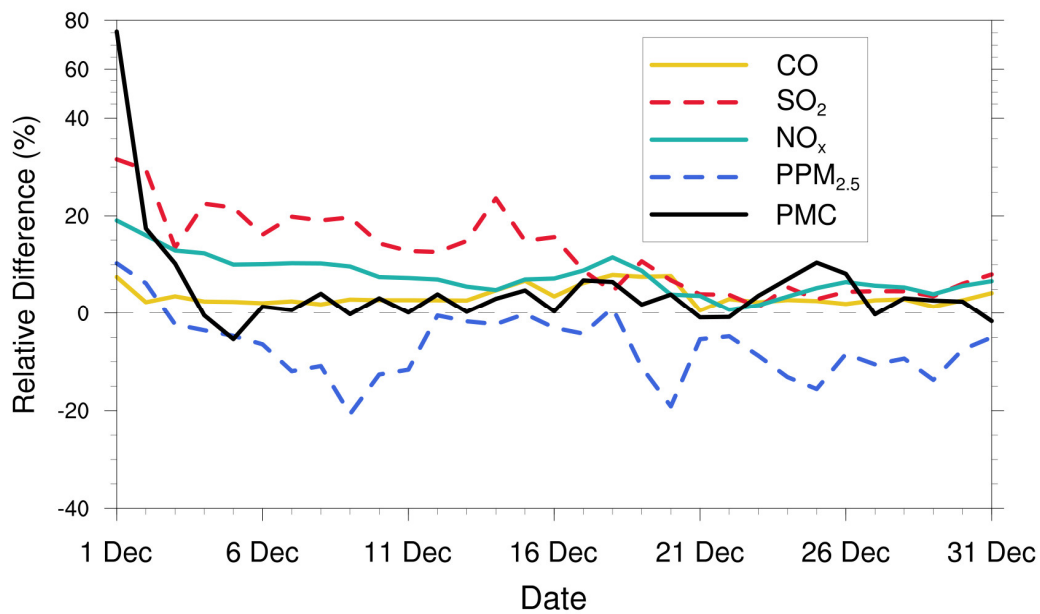
928 2016), posterior emissions (middle column), and differences (right column, posterior

929 minus prior).

930 4.3 Sensitivity tests

931 4.3.1 Impact of prior inventories

932 Various prior inventories have ~~great~~shown considerable differences in space allocation
933 and emission magnitudes. Inversion results can be sensitive to a priori emissions if the
934 observations ~~is-are~~ insufficient (Gurney et al., 2004; He et al., 2018). MEIC 2012 ~~is-was~~
935 used as an alternative a priori in EMS2 to investigate the impact of different prior
936 emissions on ~~the~~-posterior emissions. Figure 13 shows the time series of the relative
937 differences in the daily posterior emissions of the five species between the EMDA (base)
938 and EMS2 experiments. Overall, the differences between the two posterior emissions
939 gradually decreased over time. At the beginning, the differences in the CO, SO₂, NO_x,
940 PPM_{2.5}, and PMC between the two inventories (i.e., MEIC 2012 vs. MEIC 2016) ~~are~~
941 were 17.5%, 114.5%, 30.8%, 46.0%, and 72.0%, respectively, ~~while during the last ten~~
942 ~~days, the differences of the two posterior emissions have decreased~~compared to 2.5%,
943 4.5%, 4.5%, -8.9%, and 3.0%, ~~respectively in the last ten days~~. In addition, ~~it also could~~
944 ~~be found that~~ the species that has with larger emission differences at the beginning take
945 took a longer time (namely i.e. more DA steps) to achieve convergence. The quick
946 convergence of PMC emissions ~~is-was~~ attributed to the large prior uncertainty of 100%
947 used in the first ~~3~~-three DA windows. ~~Different from~~In contrast to the other species,
948 there ~~are-were~~ significant negative deviations ~~of in~~ PPM_{2.5} emissions between the two
949 experiments. ~~That This~~ may be due to the positive deviations in the precursors of PM_{2.5}
950 (i.e., SO₂ and NO_x), which ~~will~~ lead to a larger amount of secondary production. ~~To~~
951 ~~balance the total PM_{2.5} concentration, t~~The PPM_{2.5} emissions will be reduced to balance
952 the total PM_{2.5}. We compared the PM_{2.5} concentrations simulated by the two optimized
953 inventories and ~~find-found~~ that they ~~are-were~~ almost the same (Figure S6). Overall, this
954 indicates that ~~the~~-observations in China ~~is-were~~ sufficient ~~in-to~~ inferring the emissions,
955 and that our system ~~is-ratherwas~~ robust. Meanwhile, ~~it also suggests that~~ the monthly
956 posterior emissions shown in Section: 4.2 ~~are-were~~ still underestimated to a certain
957 extent.



958

959 **Figure 13.** Relative differences in CO, SO₂, NO_x, PPM_{2.5}, and PMC emissions (% the
 960 ratio of absolute difference to EMDA) between the EMDA and EMS2 experiments.

961

962 **4.3.2 Impact of prior uncertainties settings**

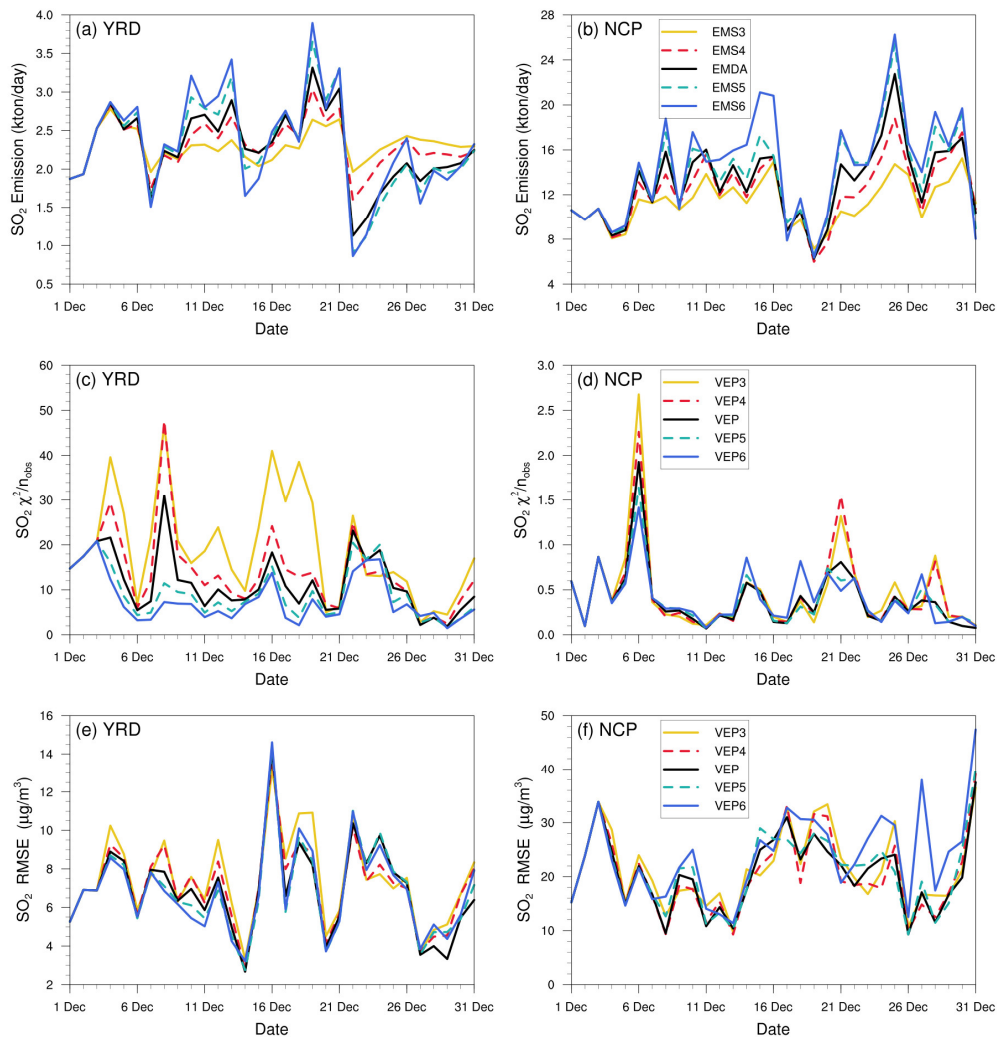
963 The uncertainty of prior emissions determines how closely the analysis is weighted
 964 towards the background and observations; ~~however, but~~ information about prior
 965 uncertainties is generally not readily available. To evaluate the possible influence of
 966 prior uncertainties on the optimized emissions, we increased/reduced the uncertainties
 967 after ~~3-three~~ days of cycling, namely starting at 0000 UTC, 3 December, by 25% and
 968 50 % in EMS3 (-50%), EMS4 (-25%), EMS5 (+25%), and EMS6 (+50%), respectively.
 969 Table 7 summarizes the emission changes with different prior ~~uncertainties-uncertainty~~
 970 settings in ~~the~~ EMS3–6 experiments. To better understand the response of the system
 971 to the emission uncertainty settings, Figure 14 ~~shows-illustrates~~ the time series of SO₂
 972 emission changes, ~~the~~ Chi-square statistics, and ~~the~~ RMSEs of simulated SO₂ with
 973 emissions updated in the EMDA and EMS3–6 experiments over the YRD and NCP
 974 (Figure 2). Compared with the EMDA, when the uncertainties ~~are~~-decreased (increased),
 975 the emissions of the ~~5-five~~ species ~~decreased~~ (increased) accordingly. ~~That-This~~ is
 976 because the posterior emissions of the ~~5-five~~ species ~~are-were~~ larger than the prior

977 emissions, and, as shown in Figure 14a–d, larger uncertainty will lead to a faster
 978 convergence, resulting in larger posterior emissions. It ~~also could~~ can also be ~~seen~~ found
 979 from Figure 14 that a faster convergence will ~~indeed~~ reduce the RMSE of the simulated
 980 concentration with the posterior emissions in the early stage of the experiment;
 981 ~~however,~~ ~~but~~ in the later stage of the experiment, there ~~are~~ ~~were~~ no significant
 982 differences ~~for~~ in the RMSE and Chi-square statistics among the different experiments.
 983 However, ~~the~~ day-to-day changes in emissions ~~can~~ also cause slight fluctuations. In
 984 addition, ~~it shows that~~ when greater uncertainties are set, the day-to-day changes in
 985 emissions are ~~also~~ more drastic, resulting in a larger RMSE, as shown in the NCP.
 986 Moreover, ~~these~~ the significant day-to-day variations ~~of~~ in the estimated emissions may
 987 not be in line with the actual situation. ~~Due~~ Owing to the spatial-temporal
 988 inhomogeneity of emissions, the differences ~~of~~ in Chi-square statistics between the
 989 YRD and NCP show that it may be necessary to apply different a priori uncertainties
 990 according to different regions (Chen et al., 2019). Therefore, when using an EnKF
 991 system for emission estimation, ~~error setting must be carefully executed~~ we have to be
 992 ~~very careful about the setting of these errors~~. Overall, the uncertainties chosen in EMDA
 993 aim to minimize the deviation of the concentration fields and maintain the stability of
 994 the inversion.

995 **Table 7.** Relative differences in CO, SO₂, NO_x, PPM_{2.5} and PMC emissions (%; the
 996 ratio of absolute difference to EMDA) between the EMDA and EMS3-6 experiments.

Species	EMS3	EMS4	EMS5	EMS6
CO	-8.6	-4	3	5.2
SO ₂	-14	-5.7	3.6	6.8
NO _x	-6.5	-3	2.8	4.5
PPM _{2.5}	-16.5	-7.8	4.6	8.7
PMC	-18.5	-8.2	7.3	13.1

997



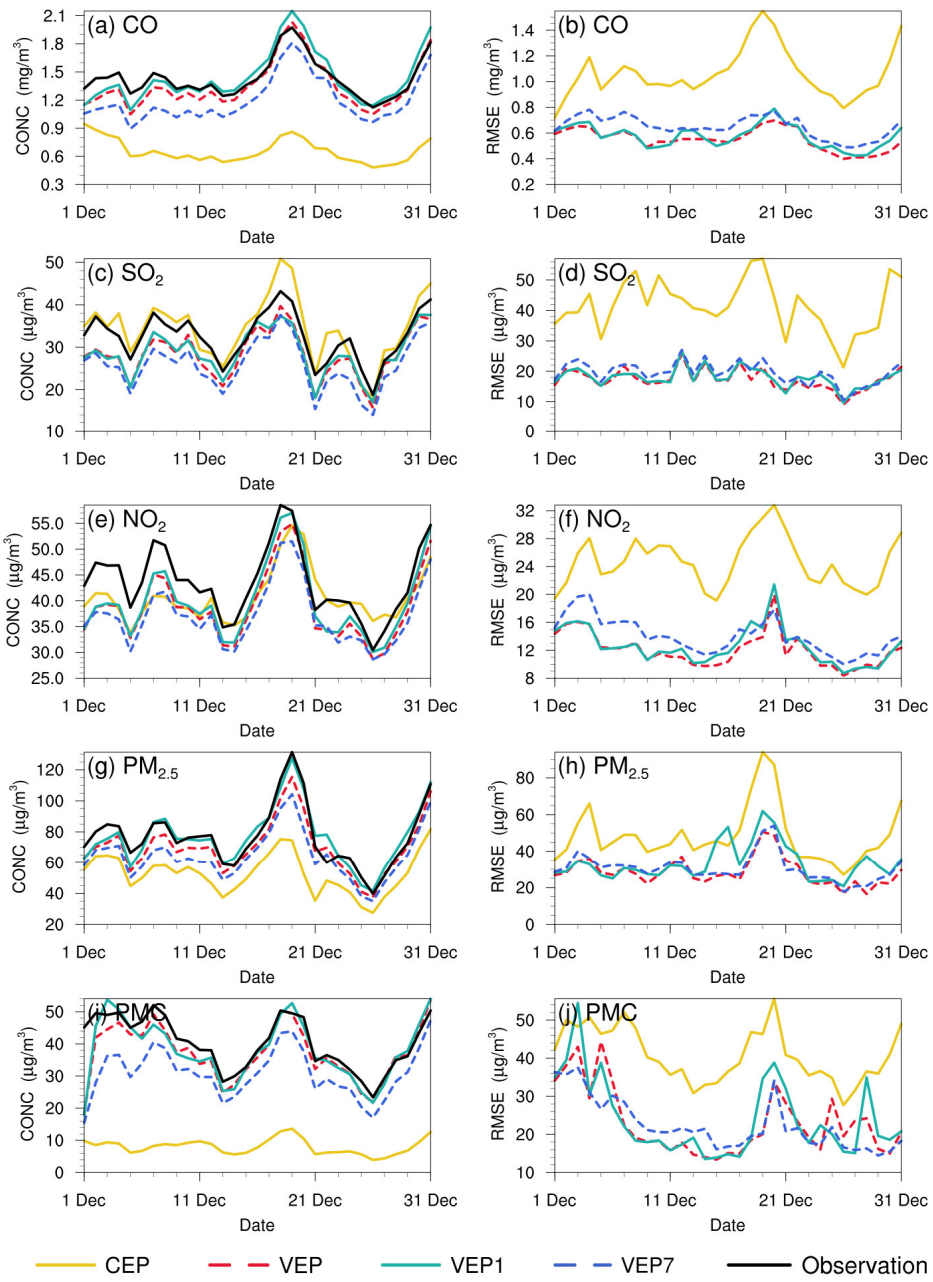
998

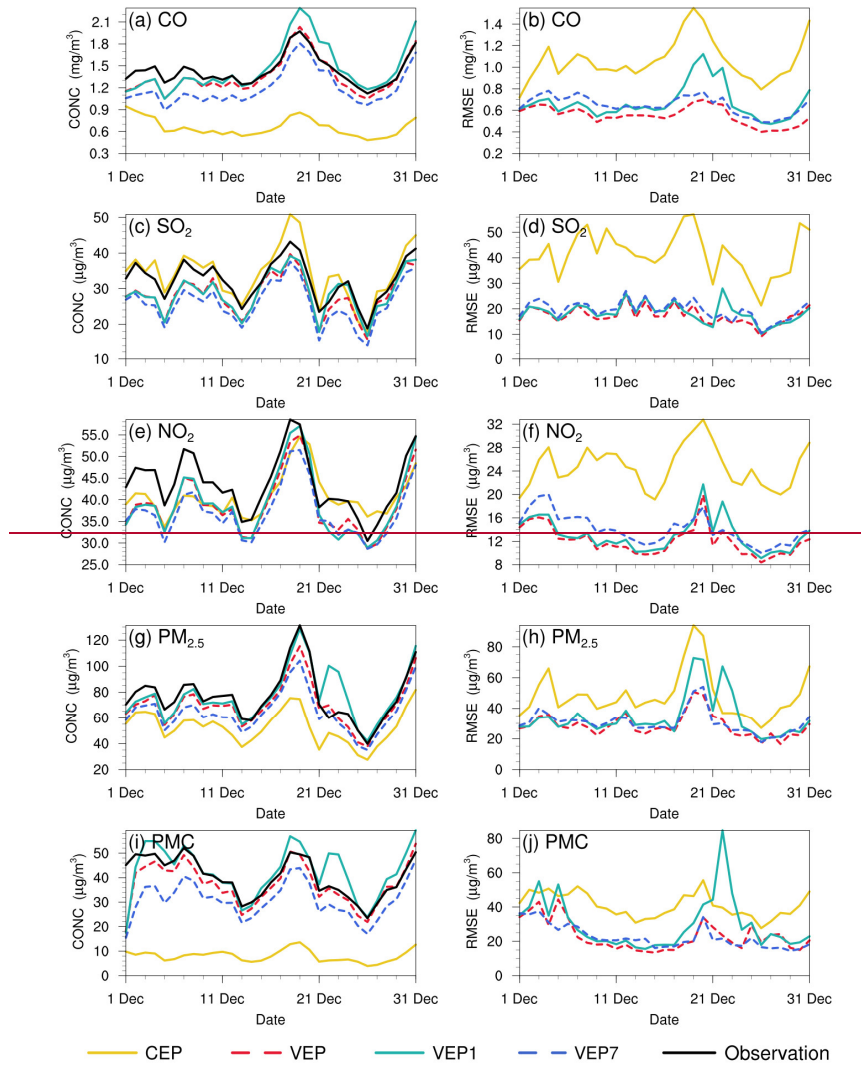
999 **Figure 14.** Time-series of SO₂ emission changes, ~~the~~ Chi-square statistics, ~~the~~
 1000 RMSE of simulated SO₂ with updated SO₂ emissions in the EMDA and EMS3-6
 1001 experiments over the ~~Yangtze River Delta (YRD)~~ and ~~North China Plain (NCP)~~.

1002 **4.3.3 Impact of observation error settings**

1003 Observation errors are aAnother factor that determines the relative weights of the
 1004 observations and background in the analysis ~~is observation errors~~. A proper estimate of
 1005 the observation error is ~~also~~ important ~~in regard to the~~for filter performance;
 1006 ~~but~~however, ~~observation errors are~~ generally not provided with ~~the~~ datasets. The
 1007 observation error is usually set to a fixed value (Ma et al., 2019), ~~a~~ specific proportion
 1008 of the observation value (Tang et al., 2013), ~~or~~ the value calculated by combining
 1009 measurement error with representative error as used in this study. Generally, the

1010 performance of ~~the~~ data assimilation is ~~quite~~ sensitive to the specification of the
1011 observation error (Tang et al., 2013). ~~To evaluate the influence of observation error on~~
1012 ~~the optimized emissions, a~~ Ssensitivity experiment (EMS7) with doubled observation
1013 error was conducted to evaluate the influence of observation error on the optimized
1014 emissions. Overall, the spatial distribution of emissions after optimization ~~is~~ was almost
1015 the same as that of the EMDA experiment, but ~~with a lower~~ the increment ~~is lower~~
1016 (Figure S7), resulting in a weaker estimate of the national total emissions s for each
1017 species. ~~This~~ is because that the observation error ~~becomes large~~ inflates and, the
1018 system ~~will be~~ becomes more ~~convinced~~ certain of the prior emission, and reduces s the
1019 effect of observation information. Figure 15 shows the time series of simulated and
1020 observed daily concentrations and their RMSEs verified against the assimilated sites.
1021 The simulations in VEP7 usually ~~perform~~ ed worse, with larger biases and RMSEs than
1022 those of VEP (Figures S8 and S9), especially in ~~most of~~ western and southern China,
1023 where posterior emissions ~~are still~~ were significantly underestimated. These results
1024 ~~usually~~ generally ~~correspond~~ ed to sluggish emission changes and large Chi-square
1025 statistics (Figure S10), suggesting that ~~too large~~ an observation error that is too large
1026 may substantially impact the estimated emissions.





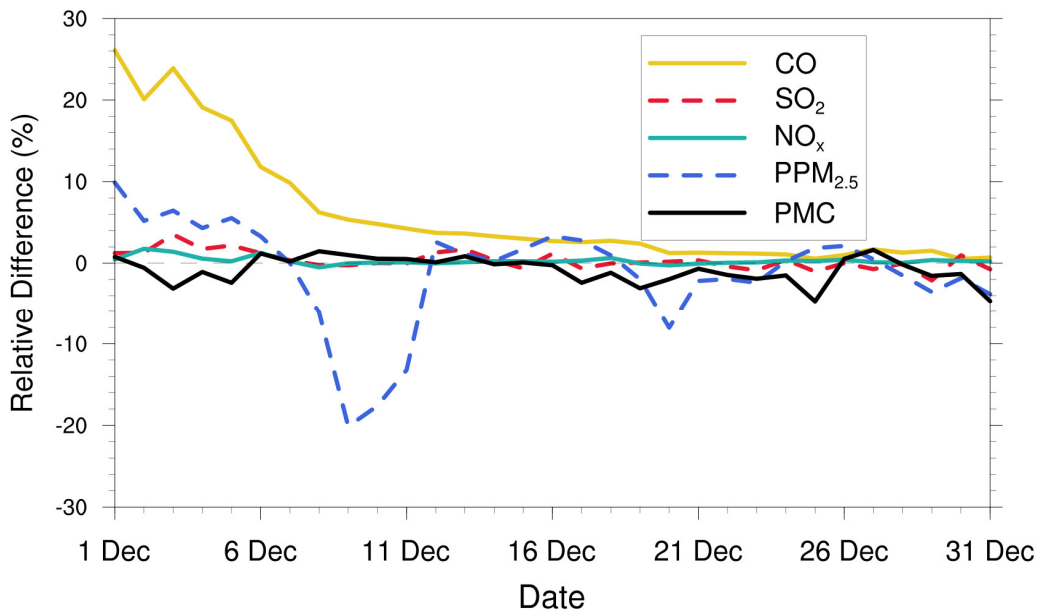
1028

1029 **Figure 15.** Time series of the daily concentrations (CONC, left) and root mean square
 1030 error (RMSE, right) obtained from CEP, VEP, VEP1, and VEP7. The simulations were
 1031 verified against the assimilated sites.

1032 4.3.4 Impact of the IC optimization of the first window

1033 ~~Many Several~~ studies ~~have shown that there would be indicate~~ large emission
 1034 discrepancies resulting from ~~the~~ IC errors (Jiang et al., 2013a; Miyazaki et al., 2017;
 1035 Tang et al., 2013), which means that if the IC is not optimized, the errors of
 1036 concentrations would be compensated for through the adjustment of emissions. To
 1037 evaluate the impact of ~~the~~ IC optimization of the first window on the emission
 1038 inversions, an the EMS8 experiment without the IA step was conducted. Figure 16
 1039 shows the time series of the relative differences in the daily posterior emissions of the

1040 five species between the EMDA and EMS8 experiments. It can be ~~found~~observed that
 1041 ~~the IC optimization of IC~~ hads ~~great~~ a significant impact on the emission inversions of
 1042 long-lived species (i.e., CO). The overall difference in the inverted CO emissions
 1043 between the two experiments ~~is about~~was approximately 5.3%, ~~and but can reach~~ 26.1%
 1044 in the first few windows, ~~the maximum difference can reach~~ 26.1%. For the short-lived
 1045 species, ~~the~~ IC optimization ~~had~~s little impact on the emissions; for example, the
 1046 average ~~d~~ emission differences of SO₂, NO_x, and PMC in the two experiments ~~are~~ were
 1047 0.3%, 0.3%, and 0.9%, respectively. For PPM_{2.5}, ~~the average emission difference~~ it is
 1048 affected not only by ~~the~~ primary emissions, but also by the complex chemistry of its
 1049 precursors. Therefore, the difference between the two experiments ~~fluctuated~~ at a
 1050 ~~certain extent~~, with overall difference of 2%. ~~It is worth noting that~~ Notably, with the
 1051 gradual disappearance of the benefit of IC assimilation, the two experiments ~~can~~
 1052 ~~reached~~ a unified state after ~~some~~ several windows. For CO, the impact of IA on
 1053 emission inversion ~~lasted~~ approximately ~~about~~ half a month. These results indicate that
 1054 removing the bias of ~~the~~ IC of the first DA window is essential for ~~the~~ subsequent
 1055 inverse analysis (Jiang et al., 2017).



1056

1057 **Figure 16.** Relative differences in CO, SO₂, ~~NO_x~~NO_x, PPM_{2.5} and PMC emissions (%
 1058 the ratio of absolute difference to EMDA) between the EMDA and EMS8.

4.3.5 Advantages of the “two-step” scheme

Adjusting the ICs and emissions simultaneously (~~i.e.~~, “one-step” scheme) has been applied to constrain prior emissions in ~~many~~ previous studies (~~e.g.~~, Evensen, 2009; Kong et al., 2019a). To investigate the impact of different methods on the optimized emissions, a sensitivity test (EMS1) was performed, in which the ICs of each DA window were ~~also~~ optimized using the ~~3DVAR-EnSRF~~ algorithm (~~Peng et al., 2018; Schwartz et al., 2014) directly~~. ~~The spatial localization radius for updating ICs was set to 90 km in horizontal and 5 layers in vertical closet to the surface with better vertical mixings. The selections of the horizontal and vertical scales were similar to Kong et al. (2021) and Tang et al. (2016). We evaluated the optimized ICs of each step, and the results showed that IC assimilation with EnSRF had good performance (Figure S11).~~

Compared with our “two-step” method (EMDA), the posterior emissions of EMS1 ~~are~~ ~~were increased by 7.9%, 9.6%, 2.7%, 27.1%, and 22.8%7%, 1.4%, 0.6%, 22.2%, and 17.2% higher~~ for CO, SO₂, NO_x, ~~PPM_{2.5}~~ and PMC, respectively (~~Figure S12~~). ~~The higher emission increase was mainly distributed in the northern China (Figure S13). Overall, there is no significant difference between the two methods for NO_x and SO₂, but for CO, it can be clearly seen that the difference increases with the inversion (Figure S11).~~ We also evaluated the posterior emissions of EMS1 (VEP1) using the ~~method described in Section 4.1.3~~. Overall, compared with EMDA, the performance of EMS1 was worse, with RMSEs of CO, SO₂, NO₂, PM_{2.5} and PMC increasing from 0.56 mg m⁻³ and 17.7, 12.3, 29.6, and 24.6 μg m⁻³ to 0.58 mg m⁻³ and 18.3, 12.9, 34.9, and 25.9 μg m⁻³, respectively (Figure 15). From the perspective of spatial distribution, the evaluation results become worse in areas where emissions increase (Figure S13). Additionally, it can be seen from the Figure 15 that the results of the VEP and VEP1 were relatively close at the beginning. However, in the heavy pollution (16–21 December) and later period, the VEP1 with “one-step” inversion emissions had higher concentrations than the observations and larger RMSE than VEP. The results verified against the independent sites showed a similar situation (Figure S8). This may be because during the period of heavy pollution, the WRF/CMAQ (offline model) did not

1088 consider the feedback process of meteorology and chemistry, resulting in low simulated
1089 values. Therefore, the system compensates for the underestimated concentrations
1090 caused by the model error through more emissions, resulting in an overestimation of
1091 emissions. The accumulation of emission errors in each independent window further
1092 leads to the overestimation of concentration after the end of high pollution, especially
1093 for species with a long lifetime (e.g. CO). In contrast, using the “two-step” inversion
1094 scheme, this overestimation will be corrected quickly in the subsequent inversion to
1095 ensure the stability of the system.

1096 As mentioned previously, in the “two-step” scheme, the unresolved posterior emission
1097 error ~~will be~~ fed back to the IC of the next window through a sufficient mixed
1098 simulation within one day for timely optimization. Meanwhile, the system **always**
1099 maintains the mass balance of the pollutants. ~~In this way~~Thus, the system updates
1100 emissions more consistently and stably. If the emission in one window is overestimated,
1101 ~~in this way~~, it ~~could~~can be compensated for in the next window with lower estimates.
1102 In contrast, when ~~the ICs are optimized assimilating with observations~~ simultaneously
1103 at each window, the overestimation will not be corrected and will accumulate to the end.
1104 (Figure S14). In addition, the assimilation for initial fields cannot be perfect (Figure
1105 S11). As shown in Figure S14, during the heavy pollution episode, there were negative
1106 biases in the optimized ICs every day, which lead to a larger positive and a smaller
1107 negative emission increment at a certain extent, and result in a larger emission in the
1108 end.

1109 To remove the effect of this imperfect initial field, we conducted another OSSE
1110 experiment (OSSE_TRUEIC) using “one-step” scheme, in which the IC of each
1111 window was directly taken from the "true" simulation. We further compared the
1112 emission error reductions between the OSSE experiment (Section 3) and the
1113 OSSE_TRUEIC experiment. The results showed that during the last ten days, the error
1114 reductions of OSSE_TRUEIC were 70.7%, 78.6%, 73.3%, 72.4%, and 63.6% for CO,
1115 SO₂, NO_x, PPM_{2.5}, and PMC, respectively, which were smaller than those in the OSSE
1116 experiment (Section 4.1.6, Figure S15), indicating that even with a perfect IC at each

1117 window, the inversion performance of “one-step” scheme was still not as good as that
1118 of the “two-step” method.We also evaluate the posterior emissions of EMS1 using the
1119 same method as shown in Sect. 4.1.3. Overall, compared to the base experiment
1120 (EMDA), the performance of EMS1 is significantly worse, with RMSEs of CO, SO₂,
1121 NO₂, PM_{2.5} and PMC increasing from 0.56 mg m⁻³, 17.7, 12.3, 29.6, and 24.6 μg m⁻³ to
1122 0.69 mg m⁻³, 18.8, 13.3, 36.8, and 33.3 μg m⁻³, respectively (Figure 15). Additionally,
1123 it can be seen from the figure that the results of the two experiments are relatively close
1124 at the beginning and during the heavy pollution period (16-21 December). However,
1125 after that, the simulated results with “one step” inversion emissions are significantly
1126 higher than the observations, and these large biases continue until the end. The results
1127 verified against the independent sites also show a similar situation (Figure S8). The
1128 reason may be that during the period of heavy pollution, the WRF-CMAQ (off line
1129 model) does not consider the feedback process of meteorology and chemistry, resulting
1130 in low simulations. Therefore, the system will compensate for the underestimated
1131 concentrations caused by the model error through more emissions, resulting in the
1132 overestimation of emissions. The accumulation of emission error in each independent
1133 window further leads to the overestimation of concentration after the end of high
1134 pollution, especially for species with a long lifetime (e.g., CO). On the contrary, this
1135 overestimation will be corrected quickly in the subsequent inversion using the “two-
1136 step” inversion scheme in this study (Figure S11), so as to ensure the stability of the
1137 system.—

1138 Additionally, as shown in section 4.3.1, with the “two-step” scheme, the differences of
1139 emissions inverted using MEIC 2012 and 2016 as a priori were only 2.5%, 4.5%, 4.5%,
1140 -8.9%, and 3.0% for CO, SO₂, NO_x, PPM_{2.5} and PMC, respectively in the last ten days.
1141 We further tested the convergence of the posterior emissions in the "one-step" inversion.
1142 the other “one step” experiment, taking MEIC 2012 as prior emissions, was conducted.
1143 However, Except for PPM_{2.5}, the relative differences of other species(Figure S12) in
1144 posterior emissions between this experiment and the EMS1 did not converge likewere
1145 slightly larger than that between EMDA and EMS2 with the “two-step” scheme (Figure

1146 ~~13S16~~), which further ~~demonstrates~~underscores the advantages of the “two-step”
1147 scheme. It should be noted that ~~the~~ model performance depends on many factors but
1148 does not affect the advantage of the “two-step” scheme in emission inversion.

1149 4.4 Discussion

1150 Optimal state estimation using an EnKF relies on the assumption of an unbiased
1151 Gaussian ~~–~~prior error, which is not guaranteed in such highly nonlinear and large biases
1152 systems. In this study, some pollutants (e.g., CO, PMC) have very large simulated
1153 biases; thus, if a small uncertainty is adopted, the emission bias cannot be fully
1154 reduced, ~~while~~ If a very large uncertainty is adopted, then the degree of freedom of
1155 adjustment is too large, and the inverted daily emissions will fluctuate abnormally.
1156 Therefore, we only set a larger prior uncertainty in the first three windows, ~~adopting~~
1157 a moderate uncertainty in the following windows, and used a “two-step” inversion
1158 scheme and cyclic iteration to gradually correct the emission errors. Figure 10(a) shows
1159 the time series of the relative differences between ~~the~~ prior and posterior emissions in
1160 each window. There ~~are~~ the were relatively large adjustments for the emissions in the
1161 first three windows, especially for PMC, but the adjustment ranges of the five species
1162 after the first ~~3~~ three windows ~~are~~ basically were within the uncertainty range (e.g., \pm
1163 25%), indicating that with this scheme, the EnKF method used in this system ~~still~~
1164 has had a good performance in emission inversion.

1165 ~~The~~ Model-data mismatch errors ~~not only comes~~ are ~~–~~ from both the emissions, ~~but~~
1166 ~~also from~~ and the inherent model errors arising from the model structure, discretization,
1167 parameterizations, and ~~the~~ biases in the simulated meteorological fields. Neglecting
1168 model errors would attribute all uncertainties to emissions, and lead to considerable
1169 biases in the estimated emissions. In the version of the CMAQ model used in this study,
1170 there ~~is~~ are no heterogeneous reactions (Quan et al., 2015; Wang et al., 2017), the
1171 parameterization scheme for the formation of secondary organic aerosols (SOA) is
1172 imperfect (Carlton et al., 2008; Jiang et al., 2012; Yang et al., 2019), no feedback
1173 between chemistry and meteorology ~~is~~ was considered, and we used an idea profile for

1174 chemical lateral boundary conditions. All ~~of~~ the above problems can lead to
1175 underestimated concentrations of pollutants, which in turn require more emissions to
1176 compensate, leading to overestimations ~~of~~ emissions. In addition, previous studies
1177 ~~have shown~~ showed that ~~the emission of~~ ammonia emissions in the MEIC inventory ~~was~~
1178 are underestimated (Kong et al., 2019b; Paulot et al., 2014; Zhang et al., 2018). ~~Due~~
1179 Owing to lack of ammonia observations, our system does not include emission
1180 estimates of ammonia, which means that the concentration of ammonium aerosol was
1181 underestimated in this system, also resulting in an overestimation ~~in~~ of the PPM_{2.5}
1182 emission. Wind-blown dust was also not simulated ~~here~~; thus, the PMC emission
1183 inverted in this system ~~do not only~~ come from anthropogenic activities, ~~but also from~~
1184 and natural sources. Although some of these shortcomings ~~could~~ can be solved ~~in the~~
1185 ~~future~~ by updating the CTM model, there will still be errors in each parameterization
1186 and ~~each~~ process. ~~Generally~~ In general, a parameter estimation method was used to
1187 reduce the model errors, in which, some uncertain parameters were included in the
1188 augmented state vector and ~~were~~ optimized synchronously based on the available
1189 observations (Brandhorst et al., 2017; Evensen, 2009). However, it is ~~still quite~~ difficult
1190 to identify the key uncertain parameters of different species in different models, which
1191 generally comes not only from the complex atmospheric chemical model, but also from
1192 hundreds of model inputs (Tang et al., 2013). Another method is bias correction, which
1193 treats the model error as a bias term, and includes it in ~~the~~ an augmented state vector
1194 (Brandhorst et al., 2017; De Lannoy et al., 2007; Keppenne et al., 2005). In addition,
1195 the weak-constraint 4D-~~Var~~ VAR method can ~~also~~ be used to reduce ~~the~~ model errors,
1196 which adds a correction term in the model integration to account for the different
1197 sources of model error (Sasaki, 1970). Although ~~the~~ reliable diagnosis of model error
1198 ~~is still remains~~ a challenge ~~at present~~ (Laloyaux et al., 2020), it should be considered in
1199 an assimilation system. In the future, ~~w~~ We will consider model errors in our system ~~in~~
1200 ~~the future~~ to obtain better emission estimates.

1201 Independent variable localization was adopted to avoid potential spurious correlations
1202 across different species in this study. However, the transmission scales for different

1203 species in different regions ~~are still different~~differ, and a more accurate localization
1204 range ~~could~~can be obtained through backward trajectory analysis. In addition,
1205 ~~Although Hamer et al. (2015) successfully used O₃ observations to estimate NO_x and~~
1206 ~~VOC emissions within the 4D var framework within an idealised model,~~ O₃
1207 observations ~~are~~were not assimilated to improve NO_x and VOC emissions using cross-
1208 species information. ~~due to the strong nonlinear effects within the O₃-NO_x-VOC~~
1209 ~~relationship (Wang et al., 2019b), in which the~~ O₃ concentration and NO_x (VOC)
1210 emissions ~~are~~were positively correlated in the NO_x (VOC)-limited region and
1211 negatively correlated in the VOC (NO_x)-limited region (Tang et al., 2011; Wang et al.,
1212 2019b). Hamer et al. (2015) successfully used O₃ observations to estimate NO_x and
1213 VOC emissions within the 4DVAR framework within an ideal model. However, the
1214 NO_x emissions are often point or line sources, which are all small compared to the
1215 model resolution. With a coarse spatial resolution, the model cannot accurately simulate
1216 the relationships between O₃ and its precursors. When assimilating O₃ observations to
1217 infer NO_x or VOC emissions, the inaccurate relationships simulated by model would
1218 worsen the inversion of NO_x emissions (Inness et al., 2015). In general, improving the
1219 model resolution can improve the detailed simulation and provide better prior
1220 information on O₃-NO_x-VOC, but it is still difficult to determine whether the condition
1221 is NO_x-limited or VOC-limited in the real atmosphere using prior emissions (Liu and
1222 Shi, 2021). Elbern et al. (2007) emphasized that assimilating O₃ to correct NO_x or VOC
1223 emissions must follow the EKMA framework derived based on observations, otherwise,
1224 even if the resolution is improved to sufficiently solve point and line sources, precursor
1225 emissions may be still adjusted in an opposite direction. In this study, the spatial
1226 resolutions of the prior emission inventory (i.e., MEIC) is 0.25° × 0.25°, which is
1227 appropriate for modeling at regional scales (Zheng et al., 2017). With this emission
1228 inventory, it is unable to accurately simulate the O₃-NO_x-VOC relationships. Therefore,
1229 to avoid the impact of inaccurate O₃-NO_x relationship on emission inversion, in our
1230 system, we did not assimilate O₃, but directly assimilate NO₂ to optimize the NO_x
1231 emissions. This work will be followed up by an ongoing work study using the available

VOC observations.

~~The initial field. Assuming that NO₂ is underestimated, the NO₂ concentration increases after assimilation, but the VOC concentration remains unchanged, then in the NO_x (VOC)-limited region, the subsequent generation of O₃ will increase (decrease); Conversely, the ozone concentration errors caused by assimilating NO₂ will also affect the subsequent NO_x emission inversion. Similarly, the model may not be able to resolve local-scale NO₂ well because of uniform distribution of concentration over the whole grid. Therefore, the model is shifted towards a NO_x (VOC)-limited regime in high (low) pollution regions, which negatively impacts results by perturbing ozone chemistry in unrealistic ways (Inness et al., 2015). Although we do not assimilate O₃ observation, model resolution still has some influence on inversion results. In our previous study (Feng et al., 2022), we have inferred the NO_x emissions over YRD in China using NO₂ observations, which has a spatial resolution of 12 km. The study period, assimilated observations, and inversion settings are the same as this study. We compared the posterior emissions of YRD between this study and Feng et al. (2022). The results showed that there was similar spatial distribution of posterior emissions inferred using the two resolutions (36 km vs 12 km) (Figure R17), but the total NO_x emission in YRD inferred using 36 km resolution was about 8.8% higher than that inferred using 12 km resolution. The differences are mainly caused by meteorological differences at different resolutions. This indicates that coarse model resolution may lead to some overestimation of the inverted emissions. To evaluate the influence of O₃-NO_x-VOC relationship change and model resolution on inversion, we also further conducted a nested emission inversion on a densely observed area (the Yangtze River Delta, China) with a grid spacing of 12 km (Feng et al., 2022). The study period is the same as this study. Results showed that the NO_x emissions in the Yangtze River Delta retrieved at two resolutions are almost the same (14.7 kt/day vs. 13.4 kt/day), with a difference of 8.8%, indicating that the emissions can be adjusted effectively by RAPAS. In addition, as shown previously, the concentrations after DA are obviously were evidently underestimated in western China, indicating that the inverted emissions over these~~

1261 regions still have large uncertainties because of the sparsity of observations, ~~which that~~
1262 are spatially insufficient for sampling the inhomogeneity of emissions. Therefore,
1263 further investigations with ~~the~~ joint assimilation of multisource observations (e.g.,
1264 satellite) are ~~also~~ underway.

~~When comparing the performances of the “two-step” and “one-step” schemes, for the
1265 “one-step” scheme, we use a combination assimilation method, namely 3DVAR for the
1266 optimizations of initial fields and EnKF for emission inversions in each DA window,
1267 which is similar as Jiang et al., (2017), but different from most previous studies
1268 (Miyazaki et al., 2017; Tang et al., 2013). Because most previous “one-step”
1269 assimilation studies used only one method (i.e., EnKF). This combination method may
1270 cause the comparison less than perfect. However, it should be noted that, even using
1271 the same method (such as EnKF) to optimize the emission of the current window and
1272 the initial field of the next window simultaneously (Peng et al., 2018), the initial field
1273 estimation errors will still be mixed in the simulated concentration field, resulting in
1274 unreasonable emission compensation in the next window. In “one-step” scheme, the
1275 essence is to build a good initial field in the high levels. Schwartz et al. (2014) compared
1276 the performances of EnKF and 3DVAR in optimizing initial fields, and found that
1277 3DVAR method can obtain a better initial field than EnKF method. Therefore, we
1278 believe that in this comparison, a combinatorial assimilation approach used in the “one-
1279 step” scheme is an acceptable approach, and the conclusion is credible, that the “two-
1280 step” scheme has better performances than the “one-step” scheme in emission estimates.~~

1282 ~~NO_xNO_x~~ is mainly emitted by transportation (Li et al., 2017), which can ~~better~~ reflect
1283 the level of economic ~~activities-activity~~ to a certain extent. Weekly emission changes
1284 were ~~also~~ explored to verify the performance of the system in depicting emission
1285 changes (Figure S1~~83~~). Although the “weekend effect” of emissions in China is not
1286 significant (Wang et al., 2014; Wang et al., 2015), the posterior ~~NO_xNO_x~~ emission
1287 changes ~~showed-are in a~~ good agreement with the observations. In our previous studies
1288 (Feng et al., 2020a; Feng et al., 2020b), ~~this~~ system was successfully applied to
1289 optimize ~~NO_xNO_x~~ and CO emissions, ~~respectively~~. The inverted emission changes

1290 were also in line with the ~~time points of~~ epidemic control time points. Additionally, the
1291 emission changes can ~~well~~ reflect the emission migration from developed ~~regions~~ or
1292 urban areas to developing ~~regions~~ or surrounding areas ~~over in~~ recent years, which ~~were~~
1293 is consistent with the emission control strategies in China. Although the system ~~does~~
1294 did not consider the model error, resulting in a certain difference between the posterior
1295 ~~emission~~ and ~~the~~ actual emissions, the spatiotemporal changes in posterior emissions
1296 ~~are were~~ relatively reasonable, ~~which~~ and can be used to monitor emission changes
1297 and ~~make inform~~ emission regulations.

1299 5 Summary and conclusions

1300 In this study, we developed a Regional multi-Air Pollutant Assimilation System
1301 (RAPASv1.0) based on the WRF/CMAQ model, 3DVAR algorithm, and EnKF
1302 algorithm. RAPAS can quantitatively optimize gridded emissions of CO, SO₂, NO_x,
1303 PPM_{2.5}, and PMC on a regional scale by simultaneously assimilating hourly *in-situ*
1304 measurements of CO, SO₂, NO₂, PM_{2.5}, and PM₁₀. This system includes two
1305 subsystems; ~~namely the~~ IA subsystem and ~~the~~ EI subsystem, which optimizes ~~the~~
1306 chemical ICs, and infers ~~the~~ anthropogenic emissions, ~~respectively~~.

1307 Taking the 2016 ~~Multi-resolution Emission Inventory for China (MEIC-2016)~~ in
1308 December as a priori, the emissions of CO, SO₂, NO_x, PPM_{2.5}, and PMC in December
1309 2016 were inferred ~~through by~~ assimilating the corresponding nationwide observations
1310 over China. The optimized ICs and posterior emissions were examined against ~~the~~
1311 assimilated and independent observations through parallel forward simulation
1312 experiments with and without DA. Sensitivity tests ~~are were also~~ performed to
1313 investigate the impact of different inversion processes, prior emissions, prior
1314 uncertainties, and observation errors on ~~the~~ emission estimates.

1315 ~~The results show that~~ RAPAS ~~showed~~ has a good performance in assimilating ground
1316 surface in situ ~~in-situ~~ observations, with the calculated emission uncertainties reduced
1317 by 44.4%, 45.0%, 34.3%, 51.8%, and 56.1% for CO, SO₂, NO_x, PPM_{2.5}, and PMC,

1318 respectively. It can also significantly improve the simulations; the RMSEs of the
1319 simulated concentrations with posterior emissions decreased by 40.1–56.3%, and the
1320 CORRs increased from 0.26–0.66 to 0.69–0.87 for different species. The OSSE
1321 experiment ~~shows~~ showed that the errors of posterior CO, SO₂, NO_x, PPM_{2.5}, and PMC
1322 could be reduced by 78.4%, 86.1%, 78.8%, 77.6%, and 72.0%, respectively. Overall,
1323 compared with the prior emissions (MEIC 2016), the posterior emissions increased by
1324 129%, 20%, 5%, and 95% for CO, SO₂, NO_x, and PPM_{2.5}, respectively. The posterior
1325 PMC emissions, which included anthropogenic and natural dust contributions,
1326 increased by 1045%. ~~The~~ sensitivity tests with different inversion processes with
1327 ~~different inversion processes show~~ revealed that the “two-step” scheme ~~in emission~~
1328 ~~inversion~~ outperformed the joint adjustment of ICs and emissions (“one-step” scheme)
1329 in emission inversion, especially after heavy pollution. ~~The~~ sensitivity tests with
1330 different prior inventories showed that the observations in China ~~is~~ were sufficient ~~in~~
1331 to inferring the emissions, and that our system ~~was~~ is less dependent on prior inventories.
1332 Additionally, ~~the~~ sensitivity tests with different prior uncertainties indicated that when
1333 the posterior emissions ~~were~~ are larger than the prior emissions, the emissions
1334 decreased/increased with the decreases/increases ~~in~~ of uncertainties because of the
1335 different convergence rates. These results demonstrate the advantage of the two-step
1336 method in emission inversion in that the inversion errors of the last window ~~can~~ could
1337 be transferred to the current window for further optimization and ~~the~~ robustness of the
1338 emissions estimated from RAPAS using ~~the~~ nationwide observations over China. It
1339 should be noted that the system usually responds slowly to too small a priori
1340 uncertainties ~~iesy~~ or too large observation errors, which may result in large errors in the
1341 estimated emissions.

1342 In summary, the comprehensive evaluation and sensitivity tests revealed that RAPAS
1343 could serve as a useful tool for accurately quantifying the spatial and temporal changes
1344 of in multi-species emissions at regional scales and near-real time, which will be helpful
1345 for ~~the~~ air pollution control in China, and ~~the~~ other regions around the world with dense
1346 ground observation networks.

1347 **Code and data availability**

1348 The codes of RAPAS v1.0 are available at <https://doi.org/10.5281/zenodo.5566225>.
1349 The WRF model code is open-source code and can be obtained from the WRF Model
1350 User's Page (<https://www2.mmm.ucar.edu/wrf/users>, last access: 25 April 2021). The
1351 CMAQ model is available through an open license as well (<https://www.epa.gov/cmaq>,
1352 last access: 25 April 2021). The observational and emission data used in this study paper
1353 are available at <https://doi.org/10.5281/zenodo.4718290> (Feng and Jiang, 2021).

1354

1355 **Author contribution**

1356 SF, FJ, ZW and ZJ developed RAPAS v1.0. SF and FJ designed the research. SF
1357 performed model simulations, analyzed data, and prepared the paper with contributions
1358 from all co-authors. FJ supervised the model development project and assisted in
1359 conceptualization and writing. HW, WH, YS, LZ, YZ, CL, and WJ contributed to the
1360 discussion and improvement of the paper.

1361

1362 **Competing interests**

1363 The authors declare that they have no conflict of interest.

1364

1365 **Acknowledgements**

1366 This work is supported by the National Key R&D Program of China (Grant No.
1367 2016YFA0600204), the National Natural Science Foundation of China (Grant No.
1368 41907378), and the Nanjing University Innovation and Creative Program for Ph.D.
1369 candidate (Grant No. CXCY19-60). We are grateful to the High Performance
1370 Computing Center (HPCC) of Nanjing University for doing the numerical calculations
1371 in this paper on its blade cluster system, and thank the MEIC team for providing the
1372 prior anthropogenic emissions (<http://www.meicmodel.org/>).

1373 **References**

- 1374 Appel, K. W., Pouliot, G. A., Simon, H., Sarwar, G., Pye, H. O. T., Napelenok, S. L., Akhtar, F., and
1375 Roselle, S. J.: Evaluation of dust and trace metal estimates from the Community Multiscale Air
1376 Quality (CMAQ) model version 5.0, Geoscientific Model Development, 6, 883-899,
1377 10.5194/gmd-6-883-2013, 2013.
- 1378 Alexe, M., Bergamaschi, P., Segers, A., Detmers, R., Butz, A., Hasekamp, O., Guerlet, S., Parker,
1379 R., Boesch, H., Frankenberg, C., Scheepmaker, R. A., Dlugokencky, E., Sweeney, C., Wofsy,
1380 S. C., and Kort, E. A.: Inverse modelling of CH₄ emissions for 2010-2011 using different
1381 satellite retrieval products from GOSAT and SCIAMACHY, Atmospheric Chemistry and
1382 Physics, 15, 113-133, 2015.
- 1383 Barbu, A. L., Segers, A. J., Schaap, M., Heemink, A. W., and Bultjes, P. J. H.: A multi-component
1384 data assimilation experiment directed to sulphur dioxide and sulphate over Europe,
1385 Atmospheric Environment, 43, 1622-1631, 2009.
- 1386 [Bocquet, M.: Parameter-field estimation for atmospheric dispersion: application to the Chernobyl](#)
1387 [accident using 4D-Var, Quarterly Journal of the Royal Meteorological Society, 138, 664-681,](#)
1388 [2012.](#)
- 1389 [Bocquet, M., Elbern, H., Eskes, H., Hirtl, M., Žabkar, R., Carmichael, G. R., Flemming, J., Inness,](#)
1390 [A., Pagowski, M., Pérez Camaño, J. L., Saide, P. E., San Jose, R., Sofiev, M., Vira, J., Baklanov,](#)
1391 [A., Carnevale, C., Grell, G., and Seigneur, C.: Data assimilation in atmospheric chemistry](#)
1392 [models: current status and future prospects for coupled chemistry meteorology models,](#)
1393 [Atmospheric Chemistry and Physics, 15, 5325-5358, 2015.](#)
- 1394 [Bocquet, M. and Sakov, P.: Joint state and parameter estimation with an iterative ensemble Kalman](#)
1395 [smoother, Nonlinear Processes in Geophysics, 20, 803-818, 2013.](#)
- 1396 Basu, S., Guerlet, S., Butz, A., Houweling, S., Hasekamp, O., Aben, I., Krummel, P., Steele, P.,
1397 Langenfelds, R., Torn, M., Biraud, S., Stephens, B., Andrews, A., and Worthy, D.: Global CO₂
1398 fluxes estimated from GOSAT retrievals of total column CO₂, Atmospheric Chemistry and
1399 Physics, 13, 8695-8717, 2013.
- 1400 Bauwens, M., Compernelle, S., Stavrou, T., Müller, J.-F., van Gent, J., Eskes, H., Levelt, P. F.,
1401 van der A, R., Veefkind, J. P., Vlietinck, J., Yu, H., and Zehner, C.: Impact of Coronavirus
1402 Outbreak on NO₂ Pollution Assessed Using TROPOMI and OMI Observations, 47,
1403 e2020GL087978, 10.1029/2020gl087978, 2020.
- 1404 Bierman: Factorization methods for Discrete Sequential estimation, Academic Press, 1977.
- 1405 Binkowski, F. S. and Roselle, S. J.: Models-3 community multiscale air quality (CMAQ) model
1406 aerosol component - 1. Model description, Journal of Geophysical Research-Atmospheres, 108,
1407 10.1029/2001jd001409, 2003.
- 1408 Brandhorst, N., Erdal, D., and Neuweiler, I.: Soil moisture prediction with the ensemble Kalman
1409 filter: Handling uncertainty of soil hydraulic parameters, Advances in Water Resources, 110,
1410 360-370, 2017.

1411 Bruhwiler, L. M. P., Michalak, A. M., Peters, W., Baker, D. F., and Tans, P.: An improved Kalman
1412 Smoother for atmospheric inversions, *Atmos. Chem. Phys.*, 5, 2691-2702, 10.5194/acp-5-
1413 2691-2005, 2005.

1414 Carlton, A. G., Turpin, B. J., Altieri, K. E., Seitzinger, S. P., Mathur, R., Roselle, S. J., and Weber,
1415 R. J.: CMAQ Model Performance Enhanced When In-Cloud Secondary Organic Aerosol is
1416 Included: Comparisons of Organic Carbon Predictions with Measurements, *Environmental
1417 Science & Technology*, 42, 8798-8802, 2008

1418 Chen, D., Liu, Z., Ban, J., and Chen, M.: The 2015 and 2016 wintertime air pollution in China: SO₂
1419 emission changes derived from a WRF-Chem/EnKF coupled data assimilation system,
1420 *Atmospheric Chemistry and Physics*, 19, 8619-8650, 10.5194/acp-19-8619-2019, 2019.

1421 Chen, D., Liu, Z., Fast, J., and Ban, J.: Simulations of sulfate-nitrate-ammonium (SNA) aerosols
1422 during the extreme haze events over northern China in October 2014, *Atmospheric Chemistry
1423 and Physics*, 16, 10707-10724, 10.5194/acp-16-10707-2016, 2016.

1424 Chevallier, F., Bréon, F.-M., and Rayner, P. J.: Contribution of the Orbiting Carbon Observatory to
1425 the estimation of CO₂ sources and sinks: Theoretical study in a variational data assimilation
1426 framework, 112, 10.1029/2006JD007375, 2007.

1427 Clements, A. L., Fraser, M. P., Upadhyay, N., Herckes, P., Sundblom, M., Lantz, J., and Solomon,
1428 P. A.: Chemical characterization of coarse particulate matter in the Desert Southwest - Pinal
1429 County Arizona, USA, *Atmospheric Pollution Research*, 5, 52-61, 10.5094/apr.2014.007, 2014.

1430 Clements, N., Hannigan, M. P., Miller, S. L., Peel, J. L., and Milford, J. B.: Comparisons of urban
1431 and rural PM_{10-2.5} and PM_{2.5} mass concentrations and semi-volatile fractions in northeastern
1432 Colorado, *Atmospheric Chemistry and Physics*, 16, 7469-7484, 10.5194/acp-16-7469-2016,
1433 2016.

1434 Daley, R.: Atmospheric Data Assimilation (gtSpecial Issue>Data Assimilation in Meteorology and
1435 Oceanography: Theory and Practice), *Journal of the Meteorological Society of Japan. Ser. II*,
1436 75, 319-329, 1997.

1437 Derber, J. C.: A VARIATIONAL CONTINUOUS ASSIMILATION TECHNIQUE, *Monthly
1438 Weather Review*, 117, 2437-2446, 1989.

1439 de Foy, B., Lu, Z., Streets, D. G., Lamsal, L. N., and Duncan, B. N.: Estimates of power plant NO_x
1440 emissions and lifetimes from OMI NO₂ satellite retrievals, *Atmospheric Environment*, 116, 1-
1441 11, 10.1016/j.atmosenv.2015.05.056, 2015.

1442 De Lannoy, G. J. M., Houser, P. R., Pauwels, V. R. N., and Verhoest, N. E. C.: State and bias
1443 estimation for soil moisture profiles by an ensemble Kalman filter: Effect of assimilation depth
1444 and frequency, 43, 2007.

1445 Ding, J., van der A, R. J., Mijling, B., Levelt, P. F., and Hao, N.: NO_x emission estimates during the
1446 2014 Youth Olympic Games in Nanjing, *Atmospheric Chemistry and Physics*, 15, 9399-9412,
1447 10.5194/acp-15-9399-2015, 2015.

1448 Elbern, H., Strunk, A., Schmidt, H., and Talagrand, O.: Emission rate and chemical state estimation

1449 by 4-dimensional variational inversion, *Atmospheric Chemistry and Physics*, 7, 3749-3769,
1450 10.5194/acp-7-3749-2007, 2007.

1451 Evensen, G.: The Ensemble Kalman Filter for Combined State and Parameter Estimation MONTE
1452 CARLO TECHNIQUES FOR DATA ASSIMILATION IN LARGE SYSTEMS, *Ieee Control*
1453 *Systems Magazine*, 29, 83-104, 10.1109/mcs.2009.932223, 2009.

1454 Feng, S., Jiang, F., Jiang, Z., Wang, H., Cai, Z., and Zhang, L.: Impact of 3DVAR assimilation of
1455 surface PM2.5 observations on PM2.5 forecasts over China during wintertime, *Atmospheric*
1456 *Environment*, 187, 34-49, 10.1016/j.atmosenv.2018.05.049, 2018.

1457 Feng, S., Jiang, F., Wang, H., Shen, Y., Zheng, Y., Zhang, L., Lou, C., and Ju, W.: Anthropogenic
1458 emissions estimated using surface observations and their impacts on PM2.5 source
1459 apportionment over the Yangtze River Delta, China, *Science of The Total Environment*, 828,
1460 154522, 2022

1461 Feng, S., Jiang, F., Wu, Z., Wang, H., Ju, W., and Wang, H.: CO Emissions Inferred From Surface
1462 CO Observations Over China in December 2013 and 2017, *Journal of Geophysical Research-*
1463 *Atmospheres*, 125, 10.1029/2019jd031808, 2020a.

1464 Feng, S., Jiang, F., Wang, H., Wang, H., Ju, W., Shen, Y., Zheng, Y., Wu, Z., and Ding, A.: NOx
1465 Emission Changes Over China During the COVID-19 Epidemic Inferred From Surface NO2
1466 Observations, *Geophysical Research Letters*, 47, 10.1029/2020gl090080, 2020b.

1467 Feng, S. and Jiang, F.: Anthropogenic air pollutant emissions over China inferred by Regional multi-
1468 Air Pollutant Assimilation System (RAPAS v1.0), Zenodo, 10.5281/zenodo.4718290, 2021.

1469 Gaspari, G. and Cohn, S. E.: Construction of correlation functions in two and three dimensions,
1470 *Quarterly Journal of the Royal Meteorological Society*, 125, 723-757, 10.1256/smsqj.55416,
1471 1999.

1472 Guenther, A. B., Jiang, X., Heald, C. L., Sakulyanontvittaya, T., Duhl, T., Emmons, L. K., and Wang,
1473 X.: The Model of Emissions of Gases and Aerosols from Nature version 2.1 (MEGAN2.1): an
1474 extended and updated framework for modeling biogenic emissions, *Geoscientific Model*
1475 *Development*, 5, 1471-1492, 10.5194/gmd-5-1471-2012, 2012.

1476 Gurney, K. R., Law, R. M., Denning, A. S., Rayner, P. J., Pak, B. C., Baker, D., Bousquet, P.,
1477 Bruhwiler, L., Chen, Y. H., Ciais, P., Fung, I. Y., Heimann, M., John, J., Maki, T., Maksyutov,
1478 S., Peylin, P., Prather, M., and Taguchi, S.: Transcom 3 inversion intercomparison: Model mean
1479 results for the estimation of seasonal carbon sources and sinks, *Global Biogeochemical Cycles*,
1480 18, 10.1029/2003gb002111, 2004.

1481 He, W., van der Velde, I. R., Andrews, A. E., Sweeney, C., Miller, J., Tans, P., van der Laan-Luijkx,
1482 I. T., Nehrkorn, T., Mountain, M., Ju, W., Peters, W., and Chen, H.: CTDAS-Lagrange v1.0: a
1483 high-resolution data assimilation system for regional carbon dioxide observations,
1484 *Geoscientific Model Development*, 11, 3515-3536, 10.5194/gmd-11-3515-2018, 2018.

1485 Hinds, W.C.: *Aerosol Technology: Properties, Behavior, and Measurement of Airborne Particles*.
1486 New York: John Wiley, 1982.

1487 Houtekamer, P. L. and Mitchell, H. L.: A sequential ensemble Kalman filter for atmospheric data
1488 assimilation, *Monthly Weather Review*, 129, 123-137, 10.1175/1520-
1489 0493(2001)129<0123:asekff>2.0.co;2, 2001.

1490 Houtekamer, P. L. and Zhang, F.: Review of the Ensemble Kalman Filter for Atmospheric Data
1491 Assimilation, *Monthly Weather Review*, 144, 4489-4532, 10.1175/mwr-d-15-0440.1, 2016.

1492 Inness, A., Blechschmidt, A. M., Bouarar, I., Chabrilat, S., Crepulja, M., Engelen, R. J., Eskes, H.,
1493 Flemming, J., Gaudel, A., Hendrick, F., Huijnen, V., Jones, L., Kapsomenakis, J., Katragkou,
1494 E., Keppens, A., Langerock, B., de Maziere, M., Melas, D., Parrington, M., Peuch, V. H.,
1495 Razinger, M., Richter, A., Schultz, M. G., Suttie, M., Thouret, V., Vrekoussis, M., Wagner, A.,
1496 and Zerefos, C.: Data assimilation of satellite-retrieved ozone, carbon monoxide and nitrogen
1497 dioxide with ECMWF's Composition-IFS, *Atmospheric Chemistry and Physics*, 15, 5275-5303,
1498 2015.

1499 Jiang, F., Liu, Q., Huang, X., Wang, T., Zhuang, B., and Xie, M.: Regional modeling of secondary
1500 organic aerosol over China using WRF/Chem, *Journal of Aerosol Science*, 43, 57-73,
1501 10.1016/j.jaerosci.2011.09.003, 2012a.

1502 Jiang, F., Zhou, P., Liu, Q., Wang, T., Zhuang, B., and Wang, X.: Modeling tropospheric ozone
1503 formation over East China in springtime, *Journal of Atmospheric Chemistry*, 69, 303-319,
1504 10.1007/s10874-012-9244-3, 2012b.

1505 Jiang, F., Wang, H. M., Chen, J. M., Machida, T., Zhou, L. X., Ju, W. M., Matsueda, H., and Sawa,
1506 Y.: Carbon balance of China constrained by CONTRAIL aircraft CO₂ measurements,
1507 *Atmospheric Chemistry and Physics*, 14, 10133-10144, 10.5194/acp-14-10133-2014, 2014.

1508 Jiang, F., Wang, H., Chen, J. M., Ju, W., Tian, X., Feng, S., Li, G., Chen, Z., Zhang, S., Lu, X., Liu,
1509 J., Wang, H., Wang, J., He, W., and Wu, M.: Regional CO₂ fluxes from 2010 to 2015 inferred
1510 from GOSAT XCO₂ retrievals using a new version of the Global Carbon Assimilation System,
1511 *Atmos. Chem. Phys.*, 21, 1963-1985, 10.5194/acp-21-1963-2021, 2021.

1512 Jiang, W., Smyth, S., Giroux, E., Roth, H., and Yin, D.: Differences between CMAQ fine mode
1513 particle and PM_{2.5} concentrations and their impact on model performance evaluation in the
1514 lower Fraser valley, *Atmospheric Environment*, 40, 4973-4985,
1515 10.1016/j.atmosenv.2005.10.069, 2006.

1516 Jiang, Z., Jones, D. B. A., Worden, H. M., Deeter, M. N., Henze, D. K., Worden, J., Bowman, K. W.,
1517 Brenninkmeijer, C. A. M., and Schuck, T. J.: Impact of model errors in convective transport on
1518 CO source estimates inferred from MOPITT CO retrievals, *Journal Of Geophysical Research-
1519 Atmospheres*, 118, 2073-2083, 2013a.

1520 Jiang, Z., Liu, Z., Wang, T., Schwartz, C. S., Lin, H.-C., and Jiang, F.: Probing into the impact of
1521 3DVAR assimilation of surface PM₁₀ observations over China using process analysis, *Journal
1522 of Geophysical Research: Atmospheres*, 118, 6738-6749, 10.1002/jgrd.50495, 2013b.

1523 Jiang, Z., Worden, J. R., Worden, H., Deeter, M., Jones, D. B. A., Arellano, A. F., and Henze, D. K.:
1524 A 15-year record of CO emissions constrained by MOPITT CO observations, *Atmospheric
1525 Chemistry And Physics*, 17, 4565-4583, 10.5194/acp-17-4565-2017, 2017.

- 1526 Jin, J., Lin, H. X., Heemink, A., and Segers, A.: Spatially varying parameter estimation for dust
 1527 emissions using reduced-tangent-linearization 4DVar, *Atmospheric Environment*, 187, 358-
 1528 373, 10.1016/j.atmosenv.2018.05.060, 2018.
- 1529 Kahnert, M.: Variational data analysis of aerosol species in a regional CTM: background error
 1530 covariance constraint and aerosol optical observation operators, *Tellus B*, 60, 2008.
- 1531 Kang, J.-S., Kalnay, E., Miyoshi, T., Liu, J., and Fung, I.: Estimation of surface carbon fluxes with
 1532 an advanced data assimilation methodology, 117, 10.1029/2012JD018259, 2012.
- 1533 Keppenne, C. L., Rienecker, M. M., Kurkowski, N. P., and Adamec, D. A.: Ensemble Kalman filter
 1534 assimilation of temperature and altimeter data with bias correction and application to seasonal
 1535 prediction, *Nonlin. Processes Geophys.*, 12, 491-503, 2005.
- 1536 Kleist, D. T., Parrish, D. F., Derber, J. C., Treadon, R., Wu, W.-S., and Lord, S.: Introduction of the
 1537 GSI into the NCEP Global Data Assimilation System, *Weather and Forecasting*, 24, 1691-1705,
 1538 10.1175/2009waf2222201.1, 2009.
- 1539 Kong, L., Tang, X., Zhu, J., Wang, Z., Pan, Y., Wu, H., Wu, L., Wu, Q., He, Y., Tian, S., Xie, Y., Liu,
 1540 Z., Sui, W., Han, L., and Carmichael, G.: Improved Inversion of Monthly Ammonia Emissions
 1541 in China Based on the Chinese Ammonia Monitoring Network and Ensemble Kalman Filter,
 1542 *Environmental Science & Technology*, 53, 12529-12538, 10.1021/acsest.9b02701, 2019a.
- 1543 Kong, L., Tang, X., Zhu, J., Wang, Z., Fu, J. S., Wang, X., Itahashi, S., Yamaji, K., Nagashima, T.,
 1544 Lee, H. J., Kim, C. H., Lin, C. Y., Chen, L., Zhang, M., Tao, Z., Li, J., Kajino, M., Liao, H.,
 1545 Sudo, K., Wang, Y., Pan, Y., Tang, G., Li, M., Wu, Q., Ge, B., and Carmichael, G. R.: Evaluation
 1546 and uncertainty investigation of the NO₂, CO and NH₃ modeling over China under the
 1547 framework of MICS-Asia III, *Atmos. Chem. Phys. Discuss.*, 2019, 1-33, 10.5194/acp-2018-
 1548 1158, 2019b.
- 1549 ~~Kurokawa, J.-i., Yumimoto, K., Uno, I., and Ohara, T.: Adjoint inverse modeling of NO_x emissions
 1550 over eastern China using satellite observations of NO₂ vertical column densities, *Atmospheric
 1551 Environment*, 43, 1878-1887, 10.1016/j.atmosenv.2008.12.030, 2009.~~
- 1552 Laloyaux, P., Bonavita, M., Chrust, M., and Gürol, S.: Exploring the potential and limitations of
 1553 weak-constraint 4D-Var, *Quarterly Journal of the Royal Meteorological Society*, 146, 4067-
 1554 4082, 2020
- 1555 Li, J.-d., Deng, Q.-h., Lu, C., and Huang, B.-l.: Chemical compositions and source apportionment
 1556 of atmospheric PM₁₀ in suburban area of Changsha, China, *Journal of Central South
 1557 University of Technology*, 17, 509-515, 2010.
- 1558 Li, M., Zhang, Q., Kurokawa, J.-i., Woo, J.-H., He, K., Lu, Z., Ohara, T., Song, Y., Streets, D. G.,
 1559 Carmichael, G. R., Cheng, Y., Hong, C., Huo, H., Jiang, X., Kang, S., Liu, F., Su, H., and Zheng,
 1560 B.: MIX: a mosaic Asian anthropogenic emission inventory under the international
 1561 collaboration framework of the MICS-Asia and HTAP, *Atmospheric Chemistry and Physics*,
 1562 17, 935-963, 10.5194/acp-17-935-2017, 2017.
- 1563 Liu, C. and Shi, K.: A review on methodology in O₃-NO_x-VOC sensitivity study, *Environmental
 1564 Pollution*, 291, 118249, 2021.

- 1565 [Liu, Y., Kalnay, E., Zeng, N., Asrar, G., Chen, Z., and Jia, B.: Estimating surface carbon fluxes based](#)
1566 [on a local ensemble transform Kalman filter with a short assimilation window and a long](#)
1567 [observation window: an observing system simulation experiment test in GEOS-Chem 10.1,](#)
1568 [Geoscientific Model Development, 12, 2899-2914, 2019.](#)
- 1569 Liu, Z., Liu, Q., Lin, H.-C., Schwartz, C. S., Lee, Y.-H., and Wang, T.: Three-dimensional variational
1570 assimilation of MODIS aerosol optical depth: Implementation and application to a dust storm
1571 over East Asia, *Journal of Geophysical Research: Atmospheres*, 116, n/a-n/a,
1572 10.1029/2011jd016159, 2011.
- 1573 Lorenc, A. C.: Modelling of error covariances by 4D-Var data assimilation, *Quarterly Journal of the*
1574 *Royal Meteorological Society*, 129, 3167-3182, 2003.
- 1575 Hamer, P. D., Bowman, K. W., Henze, D. K., Attie, J. L., and Marecal, V.: The impact of observing
1576 characteristics on the ability to predict ozone under varying polluted photochemical regimes,
1577 *Atmospheric Chemistry and Physics*, 15, 10645-10667, 2015.
- 1578 Ma, C., Wang, T., Mizzi, A. P., Anderson, J. L., Zhuang, B., Xie, M., and Wu, R.: Multiconstituent
1579 Data Assimilation With WRF-Chem/DART: Potential for Adjusting Anthropogenic Emissions
1580 and Improving Air Quality Forecasts Over Eastern China, 124, 7393-7412,
1581 10.1029/2019jd030421, 2019.
- 1582 [Meirink, J. F., Bergamaschi, P., and Krol, M. C.: Four-dimensional variational data assimilation for](#)
1583 [inverse modelling of atmospheric methane emissions: method and comparison with synthesis](#)
1584 [inversion, *Atmospheric Chemistry and Physics*, 8, 6341-6353, 2008.](#)
- 1585 Meirink, J. F., Eskes, H. J., and Goede, A. P. H.: Sensitivity analysis of methane emissions derived
1586 from SCIAMACHY observations through inverse modelling, *Atmospheric Chemistry and*
1587 *Physics*, 6, 1275-1292, 10.5194/acp-6-1275-2006, 2006.
- 1588 Maybeck: *Stochastic Models, Estimation and Control* Academic Press, 1979.
- 1589 Miyazaki, K. and Eskes, H.: Constraints on surface NO_x emissions by assimilating satellite
1590 observations of multiple species, *Geophysical Research Letters*, 40, 4745-4750,
1591 10.1002/grl.50894, 2013.
- 1592 Miyazaki, K., Eskes, H. J., and Sudo, K.: Global NO_x emission estimates derived from an
1593 assimilation of OMI tropospheric NO₂ columns, *Atmospheric Chemistry and Physics*, 12,
1594 2263-2288, 10.5194/acp-12-2263-2012, 2012a.
- 1595 Miyazaki, K., Eskes, H. J., Sudo, K., Takigawa, M., van Weele, M., and Boersma, K. F.:
1596 Simultaneous assimilation of satellite NO₂, O₃, CO, and HNO₃ data for the analysis of
1597 tropospheric chemical composition and emissions, *Atmospheric Chemistry and Physics*, 12,
1598 9545-9579, 10.5194/acp-12-9545-2012, 2012b.
- 1599 Miyazaki, K., Eskes, H., Sudo, K., Boersma, K. F., Bowman, K., and Kanaya, Y.: Decadal changes
1600 in global surface NO_x emissions from multi-constituent satellite data assimilation,
1601 *Atmospheric Chemistry and Physics*, 17, 807-837, 2017.
- 1602 [Mizzi, A. P., Edwards, D. P., and Anderson, J. L.: Assimilating compact phase space retrievals](#)

1603 [\(CPSRs\): comparison with independent observations \(MOZAIC in situ and IASI retrievals\)](#)
1604 [and extension to assimilation of truncated retrieval profiles, Geoscientific Model Development,](#)
1605 [11, 3727-3745, 2018.](#)

1606 Monteil, G., Houweling, S., Butz, A., Guerlet, S., Schepers, D., Hasekamp, O., Frankenberg, C.,
1607 Scheepmaker, R., Aben, I., and Rockmann, T.: Comparison of CH₄ inversions based on 15
1608 months of GOSAT and SCIAMACHY observations, Journal of Geophysical Research-
1609 Atmospheres, 118, 11807-11823, 2013.

1610 [Muller, J. F. and Stavrakou, T.: Inversion of CO and NO_x emissions using the adjoint of the](#)
1611 [IMAGES model, Atmospheric Chemistry and Physics, 5, 1157-1186, 2005.](#)

1612 Nassar, R., Jones, D. B. A., Kulawik, S. S., Worden, J. R., Bowman, K. W., Andres, R. J.,
1613 Suntharalingam, P., Chen, J. M., Brenninkmeijer, C. A. M., Schuck, T. J., Conway, T. J., and
1614 Worthy, D. E.: Inverse modeling of CO₂ sources and sinks using satellite observations of CO₂
1615 from TES and surface flask measurements, Atmospheric Chemistry and Physics, 11, 6029-
1616 6047, 2011.

1617 [Navon, I. M.: Practical and theoretical aspects of adjoint parameter estimation and identifiability in](#)
1618 [meteorology and oceanography, Dynamics of Atmospheres and Oceans, 27, 55-79, 1998.](#)

1619 Parrish, D. F. and Derber, J. C.: The National Meteorological Center's spectral statistical-
1620 interpolation analysis system, Monthly Weather Review, 120, 1747-1763, 10.1175/1520-
1621 0493(1992)120<1747:tnmcss>2.0.co;2, 1992.

1622 Paulot, F., Jacob, D. J., Pinder, R. W., Bash, J. O., Travis, K., and Henze, D. K.: Ammonia emissions
1623 in the United States, European Union, and China derived by high-resolution inversion of
1624 ammonium wet deposition data: Interpretation with a new agricultural emissions inventory
1625 (MASAGE_NH₃), Journal of Geophysical Research-Atmospheres, 119, 4343-4364, 2014.

1626 Peng, Z., Liu, Z., Chen, D., and Ban, J.: Improving PM_{2.5} forecast over
1627 China by the joint adjustment of initial conditions and source emissions with an ensemble
1628 Kalman filter, Atmospheric Chemistry and Physics, 17, 4837-4855, 10.5194/acp-17-4837-
1629 2017, 2017.

1630 Peng, Z., Lei, L., Liu, Z., Su, J., Ding, A., Ban, J., Chen, D., Kou, X., and Chu, K.: The impact of
1631 multi-species surface chemical observation assimilation on air quality forecasts in China,
1632 Atmospheric Chemistry and Physics, 18, 10.5194/acp-18-17387-2018, 2018.

1633 Peters, W., Jacobson, A. R., Sweeney, C., Andrews, A. E., Conway, T. J., Masarie, K., Miller, J. B.,
1634 Bruhwiler, L. M. P., Petron, G., Hirsch, A. I., Worthy, D. E. J., van der Werf, G. R., Randerson,
1635 J. T., Wennberg, P. O., Krol, M. C., and Tans, P. P.: An atmospheric perspective on North
1636 American carbon dioxide exchange: CarbonTracker, Proceedings of the National Academy of
1637 Sciences of the United States of America, 104, 18925-18930, 10.1073/pnas.0708986104, 2007.

1638 Peylin, P., Rayner, P. J., Bousquet, P., Carouge, C., Hourdin, F., Heinrich, P., Ciais, P., and
1639 contributors, A.: Daily CO₂ flux estimates over Europe from continuous atmospheric
1640 measurements: 1, inverse methodology, Atmospheric Chemistry and Physics, 5, 3173-3186,
1641 10.5194/acp-5-3173-2005, 2005.

- 1642 Purser, R. J., Wu, W. S., Parrish, D. F., and Roberts, N. M.: Numerical aspects of the application of
 1643 recursive filters to variational statistical analysis. Part I: Spatially homogeneous and isotropic
 1644 Gaussian covariances, *Monthly Weather Review*, 131, 1524-1535, 10.1175//1520-
 1645 0493(2003)131<1524:naotao>2.0.co;2, 2003.
- 1646 Quan, J., Liu, Q., Li, X., Gao, Y., Jia, X., Sheng, J., Liu, Y., 2015. Effect of heterogeneous aqueous
 1647 reactions on the secondary formation of inorganic aerosols during haze events. *Atmospheric*
 1648 *Environment* 122, 306-312.
- 1649 Rabier, F., McNally, A., Andersson, E., Courtier, P., Uden, P., Eyre, J., Hollingsworth, A., and
 1650 Bouttier, F.: The ECMWF implementation of three-dimensional variational assimilation (3D-
 1651 Var). II: Structure functions, *Quarterly Journal Of the Royal Meteorological Society*, 124,
 1652 1809-1829, 10.1256/smsqj.55002, 1998.
- 1653 Reichle, R. H., McLaughlin, D. B., and Entekhabi, D.: Hydrologic data assimilation with the
 1654 ensemble Kalman filter, *Monthly Weather Review*, 130, 103-114, 2002.
- 1655 Richardson, H., Basu, S., and Holtslag, A. A. M.: Improving Stable Boundary-Layer Height
 1656 Estimation Using a Stability-Dependent Critical Bulk Richardson Number, *Boundary-Layer*
 1657 *Meteorology*, 148, 93-109, 2013.
- 1658 Ruiz, J. and Pulido, M.: Parameter Estimation Using Ensemble-Based Data Assimilation in the
 1659 Presence of Model Error, *Monthly Weather Review*, 143, 1568-1582, 2015.
- 1660 Sarwar, G., Simon, H., Bhave, P., and Yarwood, G.: Examining the impact of heterogeneous nitryl
 1661 chloride production on air quality across the United States, *Atmospheric Chemistry and*
 1662 *Physics*, 12, 6455-6473, 10.5194/acp-12-6455-2012, 2012.
- 1663 Sasaki, Y.: SOME BASIC FORMALISMS IN NUMERICAL VARIATIONAL ANALYSIS,
 1664 *Monthly Weather Review*, 98, 875-&, 1970.
- 1665 Schneising, O., Buchwitz, M., Burrows, J. P., Bovensmann, H., Bergamaschi, P., and Peters, W.:
 1666 Three years of greenhouse gas column-averaged dry air mole fractions retrieved from satellite
 1667 - Part 2: Methane, *Atmospheric Chemistry and Physics*, 9, 443-465, 2009.
- 1668 Schwartz, C. S., Liu, Z., Lin, H.-C., and Cetola, J. D.: Assimilating aerosol observations with a
 1669 "hybrid" variational-ensemble data assimilation system, *Journal Of Geophysical Research-*
 1670 *Atmospheres*, 119, 4043-4069, 10.1002/2013jd020937, 2014.
- 1671 Sekiyama, T. T., Tanaka, T. Y., Shimizu, A., and Miyoshi, T.: Data assimilation of CALIPSO aerosol
 1672 observations, *Atmospheric Chemistry and Physics*, 10, 39-49, 10.5194/acp-10-39-2010, 2010.
- 1673 Shen, Y., Jiang, F., Feng, S., Zheng, Y., Cai, Z., and Lyu, X.: Impact of weather and emission changes
 1674 on NO₂ concentrations in China during 2014–2019, *Environmental Pollution*, 269, 116163,
 1675 10.1016/j.envpol.2020.116163, 2021.
- 1676 Shi, X. and Brasseur, G. P.: The Response in Air Quality to the Reduction of Chinese Economic
 1677 Activities During the COVID-19 Outbreak, 47, e2020GL088070, 10.1029/2020gl088070,
 1678 2020.
- 1679 Stanevich, I., Jones, D. B. A., Strong, K., Keller, M., Henze, D. K., Parker, R. J., Boesch, H., Wunch,

1680 D., Notholt, J., Petri, C., Warneke, T., Sussmann, R., Schneider, M., Hase, F., Kivi, R.,
1681 Deutscher, N. M., Velasco, V. A., Walker, K. A., and Deng, F.: Characterizing model errors in
1682 chemical transport modeling of methane: using GOSAT XCH₄ data with weak-constraint four-
1683 dimensional variational data assimilation, *Atmospheric Chemistry and Physics*, 21, 9545-9572,
1684 2021.

1685 Stavrakou, T., Müller, J.-F., Boersma, K. F., De Smedt, I., and van der A, R. J.: Assessing the
1686 distribution and growth rates of NO_x emission sources by inverting a 10-year record of NO₂
1687 satellite columns, 35, 10.1029/2008gl033521, 2008.

1688 Sun, A. Y., Morris, A., and Mohanty, S.: Comparison of deterministic ensemble Kalman filters for
1689 assimilating hydrogeological data, *Advances in Water Resources*, 32, 280-292,
1690 10.1016/j.advwatres.2008.11.006, 2009.

1691 Takagi, H., Saeki, T., Oda, T., Saito, M., Valsala, V., Belikov, D., Saito, R., Yoshida, Y., Morino, I.,
1692 Uchino, O., Andres, R. J., Yokota, T., and Maksyutov, S.: On the Benefit of GOSAT
1693 Observations to the Estimation of Regional CO₂ Fluxes, *SOLA*, 7, 161-164,
1694 10.2151/sola.2011-041, 2011.

1695 Tang, X., Zhu, J., Wang, Z. F., and Gbaguidi, A.: Improvement of ozone forecast over Beijing based
1696 on ensemble Kalman filter with simultaneous adjustment of initial conditions and emissions,
1697 *Atmospheric Chemistry And Physics*, 11, 12901-12916, 10.5194/acp-11-12901-2011, 2011.

1698 Tang, X., Zhu, J., Wang, Z. F., Wang, M., Gbaguidi, A., Li, J., Shao, M., Tang, G. Q., and Ji, D. S.:
1699 Inversion of CO emissions over Beijing and its surrounding areas with ensemble Kalman filter,
1700 *Atmospheric Environment*, 81, 676-686, 10.1016/j.atmosenv.2013.08.051, 2013.

1701 Wang, C., Lei, L., Tan, Z.-M., and Chu, K.: Adaptive Localization for Tropical Cyclones With
1702 Satellite Radiances in an Ensemble Kalman Filter, *Frontiers in Earth Science*, 8,
1703 10.3389/feart.2020.00039, 2020.

1704 Wang, H., Jiang, F., Wang, J., Ju, W., and Chen, J. M.: Terrestrial ecosystem carbon flux estimated
1705 using GOSAT and OCO-2 XCO₂ retrievals, *Atmospheric Chemistry and Physics*, 19, 12067-
1706 12082, 2019a.

1707 Wang, N., Lyu, X., Deng, X., Huang, X., Jiang, F., and Ding, A.: Aggravating O₃ pollution due to
1708 NO_x emission control in eastern China, *Science of The Total Environment*, 677, 732-744,
1709 2019b.

1710 Wang, Y. H., Hu, B., Ji, D. S., Liu, Z. R., Tang, G. Q., Xin, J. Y., Zhang, H. X., Song, T., Wang, L.
1711 L., Gao, W. K., Wang, X. K., and Wang, Y. S.: Ozone weekend effects in the Beijing-Tianjin-
1712 Hebei metropolitan area, China, *Atmospheric Chemistry and Physics*, 14, 2419-2429, 2014.

1713 Wang, Z., Li, Y., Dong, X., Sun, R., Sun, N., and Pan, L.: Analysis on weekend effect of air
1714 pollutants in urban atmosphere of Beijing, *Journal of University of Chinese Academy of
1715 Sciences*, 32, 843-850, 2015.

1716 Wang, Z., Wang, W., Tham, Y.J., Li, Q., Wang, H., Wen, L., Wang, X., Wang, T., 2017. Fast
1717 heterogeneous N₂O₅ uptake and ClNO₂ production in power plant and industrial plumes
1718 observed in the nocturnal residual layer over the North China Plain. *Atmospheric Chemistry*

1719 and Physics 17, 12361-12378.

1720 Wecht, K. J., Jacob, D. J., Sulprizio, M. P., Santoni, G. W., Wofsy, S. C., Parker, R., Boesch, H., and
1721 Worden, J.: Spatially resolving methane emissions in California: constraints from the CalNex
1722 aircraft campaign and from present (GOSAT, TES) and future (TROPOMI, geostationary)
1723 satellite observations, *Atmospheric Chemistry and Physics*, 14, 8173-8184, 2014.

1724 Wu, H., Tang, X., Wang, Z., Wu, L., Li, J., Wang, W., Yang, W., and Zhu, J.: High-spatiotemporal-
1725 resolution inverse estimation of CO and NO_x emission reductions during emission control
1726 periods with a modified ensemble Kalman filter, *Atmospheric Environment*, 236,
1727 10.1016/j.atmosenv.2020.117631, 2020.

1728 Wu, W. S., Purser, R. J., and Parrish, D. F.: Three-dimensional variational analysis with spatially
1729 inhomogeneous covariances, *Monthly Weather Review*, 130, 2905-2916, 10.1175/1520-
1730 0493(2002)130<2905:tdvaws>2.0.co;2, 2002.

1731 Yang, W., Li, J., Wang, W., Li, J., Ge, M., Sun, Y., Chen, X., Ge, B., Tong, S., Wang, Q., and Wang,
1732 Z.: Investigating secondary organic aerosol formation pathways in China during 2014,
1733 *Atmospheric Environment*, 213, 133-147, 2019.

1734 [Yumimoto, K., Uno, I., Sugimoto, N., Shimizu, A., Liu, Z., and Winker, D. M.: Adjoint inversion](#)
1735 [modeling of Asian dust emission using lidar observations, *Atmospheric Chemistry and Physics*,](#)
1736 [8, 2869-2884, 2008.](#)

1737 Zhang, F., Weng, Y., Sippel, J. A., Meng, Z., and Bishop, C. H.: Cloud-Resolving Hurricane
1738 Initialization and Prediction through Assimilation of Doppler Radar Observations with an
1739 Ensemble Kalman Filter, *Monthly Weather Review*, 137, 2105-2125, 10.1175/2009mwr2645.1,
1740 2009a.

1741 Zhang, L., Chen, Y., Zhao, Y., Henze, D. K., Zhu, L., Song, Y., Paulot, F., Liu, X., Pan, Y., Lin, Y.,
1742 and Huang, B.: Agricultural ammonia emissions in China: reconciling bottom-up and top-down
1743 estimates, *Atmospheric Chemistry and Physics*, 18, 339-355, 2018.

1744 Zhang, Q., Streets, D. G., Carmichael, G. R., He, K. B., Huo, H., Kannari, A., Klimont, Z., Park, I.
1745 S., Reddy, S., Fu, J. S., Chen, D., Duan, L., Lei, Y., Wang, L. T., and Yao, Z. L.: Asian emissions
1746 in 2006 for the NASA INTEX-B mission, *Atmospheric Chemistry and Physics*, 9, 5131-5153,
1747 10.5194/acp-9-5131-2009, 2009b.

1748 Zhang, S., Zheng, X., Chen, J. M., Chen, Z., Dan, B., Yi, X., Wang, L., and Wu, G.: A global carbon
1749 assimilation system using a modified ensemble Kalman filter, *Geosci. Model Dev.*, 8, 805-816,
1750 10.5194/gmd-8-805-2015, 2015.

1751 Zhang, X., Liu, J., Han, H., Zhang, Y., Jiang, Z., Wang, H., Meng, L., Li, Y. C., and Liu, Y.: Satellite-
1752 Observed Variations and Trends in Carbon Monoxide over Asia and Their Sensitivities to
1753 Biomass Burning, *Remote Sensing*, 12, 10.3390/rs12050830, 2020.

1754 Zheng, B., Tong, D., Li, M., Liu, F., Hong, C., Geng, G., Li, H., Li, X., Peng, L., Qi, J., Yan, L.,
1755 Zhang, Y., Zhao, H., Zheng, Y., He, K., and Zhang, Q.: Trends in China's anthropogenic
1756 emissions since 2010 as the consequence of clean air actions, *Atmospheric Chemistry And*
1757 *Physics*, 18, 14095-14111, 10.5194/acp-18-14095-2018, 2018.

1758 Zheng, B., Zhang, Q., Tong, D., Chen, C., Hong, C., Li, M., Geng, G., Lei, Y., Huo, H., and He, K.:
1759 Resolution dependence of uncertainties in gridded emission inventories: a case study in Hebei,
1760 China, Atmospheric Chemistry and Physics, 17, 921-933, 2017.